

TRACE-CLASS GAUSSIAN PRIORS FOR BAYESIAN LEARNING OF NEURAL NETWORKS WITH MCMC

TORBEN SELL AND SUMEETPAL S. SINGH

ABSTRACT. This paper introduces a new neural network based prior for real valued functions on \mathbb{R}^d which, by construction, is more easily and cheaply scaled up in the domain dimension d compared to the usual Karhunen-Loève function space prior. The new prior is a Gaussian neural network prior, where each weight and bias has an independent Gaussian prior, but with the key difference that the variances decrease in the width of the network in such a way that the resulting function is *almost surely* well defined in the limit of an infinite width network. We show that in a Bayesian treatment of inferring unknown functions, the induced posterior over functions is amenable to Monte Carlo sampling using Hilbert space Markov chain Monte Carlo (MCMC) methods. This type of MCMC is popular, e.g. in the Bayesian Inverse Problems literature, because it is stable under *mesh refinement*, i.e. the acceptance probability does not shrink to 0 as more parameters of the function's prior are introduced, even *ad infinitum*. In numerical examples we demonstrate these stated competitive advantages over other function space priors. We also implement examples in Bayesian Reinforcement Learning to automate tasks from data and demonstrate, for the first time, stability of MCMC to mesh refinement for these type of problems.

1. INTRODUCTION

Generating samples from probability measures on function spaces is both a challenging computational problem and a very useful tool for many applications, including mathematical modelling in bioinformatics [38], data assimilation in reservoir models [26], and velocity field estimation in glaciology [33], amongst many others. This paper addresses the problem of defining a computationally and statistically favourable function space prior.

In Bayesian inference on separable Hilbert spaces [46], many posterior measures μ are absolutely continuous with respect to their prior μ_0 (often a Gaussian measure, see [29] and [14], but not always, see [13], [24], and [25]), with the likelihood acting as the Radon-Nikodym derivative $d\mu/d\mu_0 \propto \mathcal{L}$. Samples from a Gaussian prior on a separable Hilbert space have a convenient expansion as the weighted sum of an infinite countable basis, weighted with independent Gaussian random variables (see (1)), which is known as the Karhunen-Loève (KL) expansion. The posteriors come with a variety of theoretical results, such as concentration inequalities and contraction rates, see e.g. [1, 29, 37, 50]. Truncating the KL expansion then reduces the problem of sampling from infinite-dimensional measures to sampling from a finite-dimensional parameter space. This truncated approximation to the true posterior gets better by including more terms of the expansion. The practical applicability of these Gaussian priors is, however, restricted to inferring unknown functions with low-dimensional domain, as the orthogonal basis required for the KL expansion results in the complexity scaling exponentially with the dimension of the unknown function's domain.

(TS) SCHOOL OF MATHEMATICS, UNIVERSITY OF EDINBURGH

(SSS) DEPARTMENT OF ENGINEERING, UNIVERSITY OF CAMBRIDGE

Key words and phrases. Bayesian Neural Networks, Value Function Estimation, preconditioned Crank Nicolson, Langevin Dynamics, Bayesian Reinforcement Learning.

Another approach to define function space priors are Bayesian Neural Networks (BNNs) [34, 35] which currently enjoy a resurgence of interest, e.g. in the machine learning community. A BNN is a random function obtained by placing a prior distribution over the weights and biases of a Neural Network (NN), with the default choice being a centered Gaussian prior on the weights with variances that scale as $\mathcal{O}(1/N^{(l)})$, where $N^{(l)}$ is the number of nodes in layer l . Some authors argue for heavy-tailed priors on the parameters, which was initially investigated in [35]. Although some theoretical results exist [32], popular criticisms include the lack of interpretability of the resulting BNNs, and recent work [53] has highlighted inter alia that novel priors are needed. Sampling approaches include Hamiltonian Monte Carlo [35], and more advanced integrators [31]. However, inference is often limited to finding the maximum-a-posteriori (MAP) estimate of the posterior [52], and the $\mathcal{O}(1/N^{(l)})$ scaling implies one cannot easily add nodes to a layer to obtain more accurate estimates: one would either have to adjust the prior variances for all nodes within the amended layer, thereby changing the prior, or not adjust the prior which results in exploding functions [32]. Other function space priors include Deep Neural Networks and Deep Gaussian Processes [12, 15], and in [15] inference is done using similar function space MCMC techniques to the ones we employ.

To calculate expectations with respect to the Bayesian posterior of the unknown function, computational methods are required as the relevant integrals are usually not analytically tractable. Two popular sampling algorithms for posteriors defined on Hilbert spaces are the preconditioned Crank-Nicolson (pCN) algorithm and its likelihood-informed counterpart the preconditioned Crank-Nicolson Langevin (pCNL) algorithm, which arise from clever (and in a way optimal) discretisations of certain stochastic differential equations [9]. These samplers are asymptotically exact and have a dimension-independent mixing rate in the sense that their proposal step size does not depend on the number of terms in the KL truncation [16, 21]. This stands in stark contrast to the well-known dimensional-dependent scaling of popular MCMC algorithms such as the Random Walk Metropolis-Hastings Algorithm and the Metropolis Adjusted Langevin Algorithm [40, 42]. Modifications of pCN include geometric [6] and likelihood-informed [10] versions. Although the computational cost can be reduced provided one knows which basis functions are informed by the data, they cannot circumvent the costly scaling in the domain dimension. This is presumably one reason why these methods have rarely been used for inferring unknown functions with domains larger than dimension two (i.e. \mathbb{R}^2) in reported examples in the literature.

This paper introduces a new neural network based prior, coined *trace-class* neural network priors, which allows for scalable (in the domain dimension) Bayesian function space inference. Hilbert space MCMC algorithms are then used to sample from the resulting posteriors, and owing to their stability under mesh-refinement, enhances the practical utility of our framework. In addition to comparisons with reported examples in the literature, we also demonstrate our technique’s usefulness on a challenging 17-dimensional Bayesian reinforcement learning example where the aim is to learn the *value function* (a function on \mathbb{R}^{17}) that can automate a task demonstrated by an expert — we combine the noisy expert data with a trace-class NN prior, through a suitably defined likelihood, to yield a Bayesian formulation.

The main contributions of this paper are as follows:

- We introduce a new *trace-class* Gaussian prior for neural networks, which is both well defined for infinite width NNs and has a degree of smoothness, and demonstrate its practical utility. The prior is independent, centred, and Gaussian across the NN’s weights and biases but is non-exchangeable over the weights within each layer and has a summable variance sequence. The latter, which gives it the trace-class

property, ensures it is a valid prior for an infinite width network, while the former results in parameters being better identified from an inference perspective. We further show that this prior is appropriate for use with Hilbert space MCMC methods (Theorem 1). The practical implications of this is that it is valid for the infinite-width limit of the NN and not just finite-dimensional projections of it (e.g. like the Random Walk Metropolis-Hastings algorithm), enjoys a dimension-independent mixing rate and, owing to the inherent scalability of neural networks to its number of inputs, is suitable for applications with high-dimensional state spaces.

- We propose a suitable likelihood for Bayesian Reinforcement Learning (BRL) for inferring the unknown continuous state value function that best describes an observed state-action data sequence. Theorem 2 and Lemma 3 justify the use of this likelihood with Gaussian prior measures on function spaces, and with our proposed neural network prior. This likelihood is also potentially of interest to the machine learning community in its own right.
- We apply Hilbert space MCMC methods to infer the unknown optimal value function in two continuous state control problems, using both our new prior and likelihood function. These exercises motivate the need for NN function priors that are, unlike a canonical orthogonal basis prior for that domain, scalable in the domain dimension, and for the first time demonstrates dimension-independent mixing of MCMC for Bayesian Inverse Reinforcement Learning.

The rest of this paper is organised as follows: In Section 2 we introduce the general inference problem, describe the canonical orthogonal basis for functions on \mathbb{R}^d , describe MCMC methods on an infinite-dimensional Hilbert space including their construction and the assumptions under which these methods are well-defined. Section 3 introduces the trace-class neural network prior and states one of our main theoretical results, showing that the proposed prior satisfies the necessary assumptions to be used with a Hilbert space MCMC algorithm. In Section 4 we formulate the Bayesian Reinforcement Learning (BRL) problem and introduce the likelihood to be used for inferring continuous state value functions from state-action data. We then show that the likelihood satisfies the assumptions needed to be admissible in a Hilbert space MCMC setting. Finally, Section 5 provides numerical results for the proposed prior and the likelihood for different control problems. Proofs can be found in the appendix.

1.1. Notation. We use curly letters (\mathcal{X} and \mathcal{A}) for spaces and sets. Subscripts denote both the temporal and spatial variables, but it will be clear from the context which one is being referred to. Φ denotes the Gaussian cumulative distribution function (cdf), ϕ the Gaussian probability density function (pdf). φ is used for basis functions, ζ denotes an activation function. The likelihood function we will write as \mathcal{L} , the log-likelihood as ℓ , and T is the number of data points used in the likelihood. ℓ^2 will also denote the space of square-summable sequences. The space of square-integrable functions, with respect to the Lebesgue measure, from $\mathcal{X} \subseteq \mathbb{R}^d$ to \mathbb{R} is denoted $L^2(\mathcal{X}, \mathbb{R})$ or simply L^2 . For the control problem, \mathcal{T} denotes the deterministic state dynamics, mapping a state-action pair (x, a) to the next state x' . The value function is denoted with the letter v .

2. PROBLEM FORMULATION

The objective is to sample from a target distribution μ defined over an infinite-dimensional separable Hilbert space. The targets of interest in this work are Bayesian posterior distributions arising from a Gaussian prior measure μ_0 and a likelihood which can be evaluated point wise. One such likelihood is the Gaussian likelihood that arises from observations of

a solution to a PDE with additive Gaussian noise given in Section 3.3, which is a standard likelihood in the Bayesian Inverse problems literature [46]. The other likelihood we will work with is one for continuous state control problems which is introduced in Section 4. In what follows, we will assume that the posterior has a density with respect to the prior, in which case the Radon-Nikodym derivative is well defined and is proportional to the likelihood. The posterior density with respect to the prior is given by $\frac{d\mu}{d\mu_0}(u) = \frac{1}{Z} \exp(\ell(y|u))$, where y are observations, ℓ is the log-likelihood, and $Z = \int \exp(\ell(y|u))\mu_0(du) > 0$ is the normalisation constant.

For an infinite-dimensional separable Hilbert space \mathcal{H} , say $\mathcal{H} = L^2(\mathcal{X}, \mathbb{R})$ to frame the discussion in this section (and later in Section 3 the sequence space $\mathcal{H} = \ell^2$), there exists an orthonormal basis $\{\varphi_i\}_{i=1}^{\infty}$ such that any element $u \in \mathcal{H}$ can be obtained as the limit $u(x) = \lim_{N \rightarrow \infty} \sum_{i=1}^N a_i \varphi_i(x)$, where $a_i = \langle u, \varphi_i \rangle_{\mathcal{H}}$ with $\langle u, \varphi_i \rangle_{\mathcal{H}}$ denoting the inner product on \mathcal{H} . Let the prior $\mu_0 = \mathcal{N}(0, \mathcal{C})$ be a Gaussian measure on \mathcal{H} . If the operator \mathcal{C} is trace-class with orthonormal eigenvalue-eigenfunction pairs $(\lambda_i^2, \varphi_i(x))$, $i = 1, 2, \dots$, one can sample from μ_0 by sampling a sequence of $\xi_i \sim \mathcal{N}(0, \lambda_i^2)$ and by then defining

$$(1) \quad u(x) = \sum_{i=1}^{\infty} \xi_i \varphi_i(x).$$

The sum defines $u(x) \in \mathcal{H}$ almost surely and is the Karhunen-Loève (KL) expansion [20]. One may thus think of a sample from the Gaussian measure as the sum of a sequence of 1-dimensional Gaussians with summable variances. This allows us to truncate the series expansion such that we have N active terms, with the remainder, or approximation error, tending to zero as N increases:

$$u(x) = \sum_{i=1}^N \xi_i \varphi_i(x) + \sum_{i=N+1}^{\infty} \xi_i \varphi_i(x)$$

$$\|u(x) - \sum_{i=1}^N \xi_i \varphi_i(x)\|^2 = \sum_{i=N+1}^{\infty} \|\xi_i \varphi_i(x)\|^2 = \sum_{i=N+1}^{\infty} \xi_i^2 < \infty \quad \text{a.s..}$$

Other more elaborate truncation schemes are discussed in [9], but we will focus on a fixed number of terms for computational and notational convenience. For some applications, φ_i for large i can be interpreted as high-oscillating functions which may not be discernible by the observation operator, see the example in Section 3.3 or Figure 1, where the large i coefficients are responsible for the oscillating function in the left panel, and forced to 0 on the right. Note that, given some $u \in \mathcal{H}$, we can let u' be u with i -th component set to 0, i.e. $u' = u - \langle u, \varphi_i \rangle \varphi_i$. It follows from Assumption 4 (stated later in the manuscript) that $\lim_{i \rightarrow \infty} \ell(y|u') = \ell(y|u)$, for any $u \in \mathcal{H}$. Following the approach of [46, Theorem 4.6] this closeness of the likelihoods $\ell(y|u)$ and $\ell(y|u - \langle u, \varphi_i \rangle \varphi_i)$ translates to closeness of the corresponding posteriors.

We emphasise that the above discussion holds not only for the space $\mathcal{H} = L^2(\mathcal{X}, \mathbb{R})$, which is predominantly how it is applied in [5, 6, 9], but also for $\mathcal{H} = \ell^2$ (with the only change being the choice of the orthonormal basis), which will be of particular importance in this paper. In infinite-dimensional spaces, one has to be careful to ensure the posterior is well defined, see [46] for a discussion on Gaussian priors and likelihoods given through possibly non-linear mappings, observed in Gaussian noise. We will work with the following assumptions, which we prove are satisfied for the likelihood defined in Section 4.

- (1) μ_0 is a Gaussian prior defined on a separable Hilbert space \mathcal{H} , with a trace-class covariance operator \mathcal{C} , that is, the eigenvalues λ_i^2 corresponding to the eigenfunctions φ_i satisfy $\sum_i \lambda_i^2 < \infty$;
- (2) The posterior is well-defined, i.e. the integral of the likelihood with respect to the prior is positive and finite.

2.1. A canonical approximation for functions on \mathbb{R}^d . Consider a d -dimensional hypercube $\mathcal{X} = [0, 1]^d$, the Hilbert space $\mathcal{H} = L^2(\mathcal{X}, \mathbb{R})$, and a Gaussian prior measure μ_0 on \mathcal{H} . A Bayesian approach entails choosing the covariance matrix \mathcal{C} for the Gaussian prior μ_0 , and we discuss a standard choice below. If the problem requires it, as in Section 3.3 where a PDE is solved, it is possible to choose \mathcal{C} such that the samples are almost surely differentiable.

Given eigenvalues λ_i and basis functions φ_i for a 1-dimensional function, one approach to scale this basis up to a d -dimensional domain is by taking a tensor product of the basis, see e.g. [27] for the multivariate Fourier basis, or [54] for Wavelets and other basis expansions. For the KL expansion, we thus get, for a multi-index $k = (k_1, \dots, k_d) = k_{1:d}$ with $k_i = 1, \dots, N$,

$$(2) \quad u(x) = \sum_k \xi_k \varphi_k(x) = \sum_{k_1=1}^N \cdots \sum_{k_d=1}^N \left[\xi_{k_{1:d}} \prod_{j=1}^d \varphi_{k_j}(x_j) \right],$$

where $\xi_{k_{1:d}} \sim \mathcal{N}(0, \lambda_{k_{1:d}}^2)$ with $\lambda_{k_{1:d}}$ being a function of the respective eigenvalues λ_{k_i} capturing the correlation between dimensions. In total, there are N^d active terms, that is, the complexity is exponential in the dimension d . This will be computationally prohibitively expensive, even for moderately small d . An approximation-theoretic argument for the exponential scaling has been made by [2], who showed that a Sobolev function u on a d -dimensional domain with smoothness α can be approximated in L^2 within ϵ error using N_ϵ basis terms, where $N_\epsilon \propto \epsilon^{-d/\alpha}$. To circumvent the exponential growth of terms in the domain dimension, one could employ the following simplifications with only mixed partials up to order two [45]

$$(3) \quad u(x) \approx \sum_{i=1}^d u_i(x_i) + \sum_{i=1}^d \sum_{j=i+1}^d u_{i,j}(x_i, x_j),$$

with $dN + \frac{d(d-1)}{2}N^2$ coefficients to be estimated, thus still achieving a significant reduction compared to N^d terms before. In our numerical work, this approximation is an obvious candidate to contrast against.

With the approximation (3) in mind, one restricts oneself to the prior on finitely many random functions u_i and $u_{i,j}$, each of which themselves is sampled from a Gaussian measure $\mathcal{N}(0, \mathcal{C}_1)$, or $\mathcal{N}(0, \mathcal{C}_2)$, respectively. One identifies each of these functions with their Karhunen-Loève expansion

$$(4) \quad u_i(x_i) = \sum_{k=1}^{\infty} \xi_{i,k} \varphi_k(x_i), \quad u_{i,j}(x_i, x_j) = \sum_{k=1}^{\infty} \xi_{i,j,k} \psi_k(x_i, x_j)$$

where the φ_k and ψ_k are the eigenfunctions corresponding to the eigenvalues $\lambda_{\varphi,k}^2$ and $\lambda_{\psi,k}^2$, respectively. The $\xi_{i,k}$ and $\xi_{i,j,k}$ are independent normal random variables $\xi_{i,k} \sim \mathcal{N}(0, \lambda_{\varphi,k}^2)$ and $\xi_{i,j,k} \sim \mathcal{N}(0, \lambda_{\psi,k}^2)$. As before one requires the covariance operators to be *trace-class*, and truncates the expansion (4) after a finite number of term.

The numerical experiments using the KL function space prior in this paper are based on the following Fourier basis functions, φ_k defined on $[0, 1]$, $\psi_k = \psi_{k_1, k_2}$ defined on $[0, 1]^2$ and

indexed by a double index $k = (k_1, k_2) \in \mathbb{N} \times \mathbb{N}$:

(5)

$$\begin{aligned} \varphi_{2k}(x_i) &= \sin(2\pi k x_i) & \varphi_{2k+1}(x_i) &= \cos(2\pi k x_i) \\ \psi_{2k_1, 2k_2}(x_i, x_j) &= \sin(2\pi k_1 x_i) \sin(2\pi k_2 x_j) & \psi_{2k_1+1, 2k_2}(x_i, x_j) &= \cos(2\pi k_1 x_i) \sin(2\pi k_2 x_j) \\ \psi_{2k_1, 2k_2+1}(x_i, x_j) &= \sin(2\pi k_1 x_i) \cos(2\pi k_2 x_j) & \psi_{2k_1+1, 2k_2+1}(x_i, x_j) &= \cos(2\pi k_1 x_i) \cos(2\pi k_2 x_j), \end{aligned}$$

for $i \neq j$, with corresponding eigenvalues

$$(6) \quad \lambda_{\varphi, 2k}^2 = \lambda_{\varphi, 2k+1}^2 = \frac{1}{k^\alpha}$$

$$(7) \quad \lambda_{\psi, 2k_1, 2k_2}^2 = \lambda_{\psi, 2k_1+1, 2k_2}^2 = \lambda_{\psi, 2k_1, 2k_2+1}^2 = \lambda_{\psi, 2k_1+1, 2k_2+1}^2 = \frac{1}{(\sqrt{k_1^2 + k_2^2})^\alpha}.$$

See Figure 1 for some representative draws from this prior, which is a modification from the prior used in Section 4.2 of Beskos et al. (2017). The covariance operator is of the form $-\Delta^{-\alpha}$ where Δ denotes the Laplacian, and we allow both Dirichlet (e.g. $\varphi_{2k}(0) = \varphi_{2k}(1) = 0$) and Neumann boundary conditions (e.g. $\varphi'_{2k+1}(0) = \varphi'_{2k+1}(1) = 0$), with opposing sides of the square $[0, 1]^2$ satisfying the same boundary conditions.

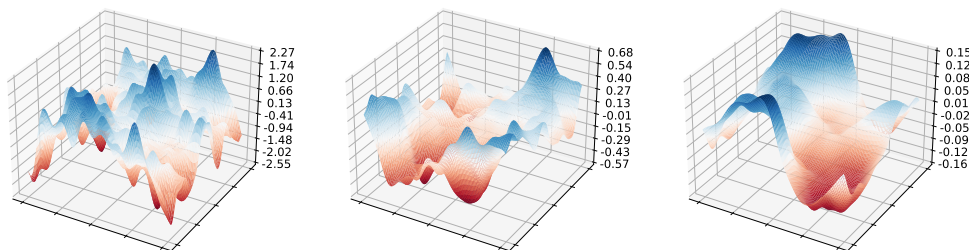


FIGURE 1. Three samples from the Karhunen-Loève prior; the basis functions are the two-dimensional Fourier functions. In ascending order from left to right we set $\alpha \in \{1.001, 1.5, 2\}$ with the eigenvalues scaling as $\lambda_k^2 \propto 1/(k_1^2 + k_2^2)^\alpha$, for the double index $k = (k_1, k_2)$. The tuning parameter α controls the smoothness of the samples.

Section 3 will introduce a prior which scales favourably with the domain-dimension as it does not require pre-defining an orthogonal basis.

2.2. Metropolis-Hastings algorithms on Hilbert spaces. This section recapitulates how to define ‘sensible’ Metropolis-Hastings Markov chain Monte Carlo algorithms for inference over the ξ_i in (1). Using Markov chains is an established approach to sample from distributions on finite-dimensional state spaces (see [8] for an overview of MCMC methods) and our emphasis here is to review algorithms which can theoretically deal with arbitrarily many basis coefficients, without having to be re-tuned to avoid the usual problem of the acceptance probability degenerating as one includes more coefficients. This property, known as *stability under mesh-refinement*, is not satisfied by the popular Random Walk Metropolis-Hastings Algorithm (RWMH, [22]), or by the Metropolis Adjusted Langevin Algorithm (MALA, [41]).

Two algorithms which are both dimension-independent are the preconditioned Crank-Nicolson (pCN) and the preconditioned Crank-Nicolson Langevin (pCNL) algorithms, the former introduced as early as [36] and both derived and discussed in [9]. Motivated by the idea of increasing dimensions translating to evaluating a function on a finer mesh, we will also refer to the dimension-independence of these algorithms as stability under mesh-refinement. Both algorithms can be seen as a discretisation of the following stochastic partial differential equation:

$$(8) \quad \frac{du}{ds} = -\mathcal{K}(\mathcal{C}^{-1}u - \gamma D\ell(u)) + \sqrt{2\mathcal{K}} \frac{dB}{ds},$$

where $D\ell$ is the Fréchet derivative of the log-likelihood¹, \mathcal{K} is a preconditioner, \mathcal{C} is the covariance operator of the Gaussian prior measure, B is a Brownian motion, and γ a tuning parameter: if $\gamma = 0$, the invariant distribution of (8) is the prior μ_0 , and for $\gamma = 1$ the invariant distribution is the posterior μ . With the choice $\mathcal{K} = \mathcal{C}$ (the preconditioned case, such that the dynamics are scaled to the prior variances), discretising (8) using a Crank-Nicolson scheme results in pCN (for $\gamma = 0$) and pCNL (for $\gamma = 1$). The resulting discretisations can be simplified to

$$(9) \quad v = \sqrt{1 - \beta^2}u + \beta w, \quad w \sim \mathcal{N}(0, \mathcal{C}), \quad (\text{pCN})$$

$$(10) \quad v = \frac{1}{2 + \delta} \left[(2 - \delta)u + 2\delta\mathcal{C}D\ell(u) + \sqrt{8\delta}w \right], \quad w \sim \mathcal{N}(0, \mathcal{C}), \quad (\text{pCNL})$$

for step sizes $\beta \in (0, 1]$ and $\delta \in (0, 2)$, respectively. Note that due to the discretisation scheme used, pCN is prior-reversible, and using it as a proposal in a Metropolis-Hastings sampler to target the posterior, the proposal is accepted with probability $\min\{1, \exp(-\ell(u) + \ell(v))\}$. If the pCNL dynamics are used as a proposal for a MH scheme, the acceptance probability is given by $\min\{1, \exp(\rho(u, v) - \rho(v, u))\}$ where

$$\rho(u, v) = -\ell(u) - \frac{1}{2}\langle v - u, \mathcal{D}\ell(u) \rangle - \frac{\delta}{4}\langle u + v, \mathcal{D}\ell(u) \rangle + \frac{\delta}{4}\|\sqrt{\mathcal{C}}\mathcal{D}\ell(u)\|^2.$$

Both pCN and pCNL are such that, for an uninformative likelihood, all moves are accepted. In practice, the likelihood Assumptions 3 and 4 ensure that, unlike RWMH or MALA, neither pCN nor pCNL require their step size β or δ to go to 0 as one includes more coefficients in the KL expansions [9].

To conclude this section, we state the assumptions under which both pCN [9, Thm 6.2] and pCNL are well defined. Assumptions 3 and 4 [9, Assumptions 6.1] are needed for both pCN and pCNL, while 5 is only required for pCNL [6]:

- (3) There exist constants $K > 0$, $p > 0$ such that $0 \leq -\ell(y|u) < K(1 + \|u\|_{\mathcal{H}}^p)$ holds for all $u \in \mathcal{H}$.
- (4) For all $r > 0$, $\exists K(r) > 0$ such that for all u, v with $\max(\|u\|_{\mathcal{H}}, \|v\|_{\mathcal{H}}) < r$, we have $|\ell(y|u) - \ell(y|v)| \leq K(r)\|u - v\|_{\mathcal{H}}$.
- (5) For all $u \in \mathcal{H}$, $\mathcal{C}D\ell(u) \in \text{Im}(\mathcal{C}^{1/2})$, μ_0 -almost surely. That is, for any draw u from the prior, the *preconditioned* differential operator at u is in the Cameron-Martin space of the prior with probability 1.

¹Note that we use the log-likelihood ℓ rather than the potential $\Phi = -\ell$ as the authors of [9].

3. TRACE-CLASS NEURAL NETWORK PRIORS

The Gaussian prior on $\mathcal{H} = L^2(\mathcal{X}, \mathbb{R})$ exploits the isometry between the function space $L^2(\mathcal{X}, \mathbb{R})$ and the sequence space ℓ^2 using the Karhunen-Loève expansion [20], but the computational complexity of using a basis-expansion on a high-dimensional domain is unfeasible even when using approximate function representations such as in [45].

Neural networks have been shown to have excellent empirical performance in high-dimensional function regression tasks. Bayesian neural networks (BNNs), capitalising on this success, randomise the neural network architecture to yield Bayesian priors for functions. BNNs are popular as they empirically show good results, scale well in the dimension of the function’s domain, and more ground is being made on the supporting theory, e.g. on their approximation quality, infinite-width behaviour etc [23, 32]. A drawback of standard BNNs is currently the limited interpretability of the posterior distributions on the parameter space, as the distribution on each weight degenerates due to the scaling of the variance proportional to the number of nodes.

We now propose a prior for the parameters that define a neural network which will generate almost surely well-defined functions for an infinite-width neural network. This is achieved by parameterising the infinite width neural network using sequences in the Hilbert space $\mathcal{H} = \ell^2$, the space of square-summable real valued sequences, and endow it with a trace-class Gaussian prior. This then allows inference for such neural networks to be conducted using the dimension-independent MCMC methods discussed in Section 2.2.

Through the architecture of the neural network, the prior μ_0 over the parameters implicitly defines a prior on the output function of the neural network. Under mild assumptions on the network architecture, and if \mathcal{X} is compact, the output functions, which we denote as v , are μ_0 -almost surely square-integrable over \mathcal{X} , and the prior thus naturally defines a prior over $L^2(\mathcal{X}, \mathbb{R})$ as well. Neural network priors are also more flexible compared to the Karhunen-Loève expansion of a Gaussian measure: one neither needs to specify a covariance operator and find its eigenfunctions, nor decide on a basis which is then used to define a Gaussian prior. By giving up the orthogonality of these eigenfunctions (which allow for a rich theoretical analysis), one gains on the performance side, see our numerical comparisons in Section 5.3. We coin the term *trace-class neural network prior* (tcNN) to emphasise that the prior leads to a well-defined function space prior if the variances of all parameters are appropriately summable. The term is well-established for Gaussian measures, where these are called trace-class if the eigenvalues of the covariance operator are summable.

Consider a n -layer feed-forward fully-connected neural network illustrated in Figure 2. The width of layer l is $N^{(l)}$, the input to the first layer is $x \in [0, 1]^d$, the domain of the function to be approximated, and let $v(x) = f_1^{(n+1)}(x) \in \mathbb{R}$ denote the network’s output; for notational convenience we write $N^{(0)} = d$ and $N^{(n+1)} = 1$. The network is described fully by the following set of real valued weights and biases,

$$(11) \quad w = \left\{ w_{i,j}^{(l)} \right\}_{i=1,j=1,l=1}^{N^{(l)}, N^{(l-1)}, n+1}, \quad b = \left\{ b_i^{(l)} \right\}_{i=1,l=1}^{N^{(l)}, n+1}, \quad \theta = (w, b),$$

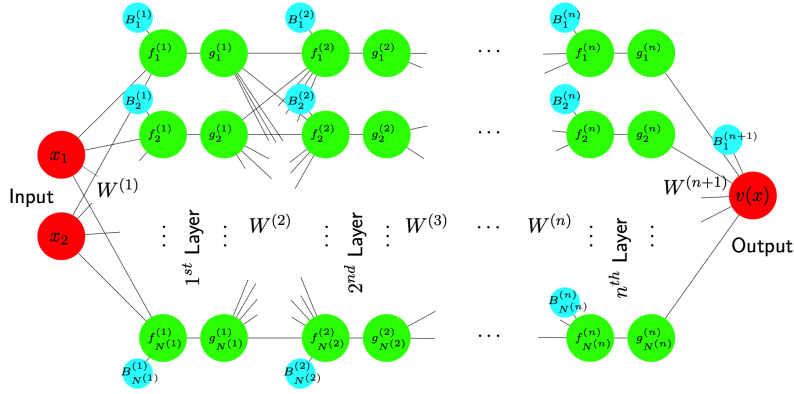


FIGURE 2. A n -layer feed-forward neural network defining a function $v : \mathbb{R}^2 \rightarrow \mathbb{R}$. Note that $g_i^{(l)} = \zeta(f_i^{(l)})$.

where we have summarised w and b as θ . Given an *activation function* $\zeta : \mathbb{R} \rightarrow \mathbb{R}$, the functions of each layer are

$$\begin{aligned}
 f_i^{(1)}(x) &= b_i^{(1)} + \sum_{j=1}^d w_{i,j}^{(1)} x_j, \quad i = 1 \dots N^{(1)} \\
 f_i^{(l)}(x) &= b_i^{(l)} + \sum_{j=1}^{N^{(l-1)}} w_{i,j}^{(l)} \zeta(f_j^{(l-1)}(x)), \quad i = 1 \dots N^{(l)}, \quad l = 2 \dots n \\
 v(x) &= f_1^{(n+1)}(x) = b_1^{(n+1)} + \sum_{j=1}^{N^{(n)}} w_{1,j}^{(n+1)} \zeta(f_j^{(n)}(x)).
 \end{aligned}
 \tag{12}$$

The prior μ_0 is now defined as follows: the individual weights and biases in each layer l are independent and normally distributed, and we emphasise here that the novelty is to choose the variances not uniformly, but to decrease them as one moves into the tail nodes of each layer:

$$W_{i,j}^{(1)} \sim \mathcal{N}\left(0, \frac{\sigma_w^{(1)}}{i^\alpha}\right), \quad W_{i,j}^{(l)} \sim \mathcal{N}\left(0, \frac{\sigma_w^{(l)}}{(ij)^\alpha}\right) \text{ for } l = 2 \dots n+1, \quad B_i^{(l)} \sim \mathcal{N}\left(0, \frac{\sigma_b^{(l)}}{i^\alpha}\right),
 \tag{13}$$

where indices i , j , and l are defined in (11), $\alpha > 1$ is a fixed constant, and $\sigma_w^{(l)} > 0$ for each l (to avoid degeneracy of the prior). The reader should note that the prior is invariant with respect to permutation of the input variables, thus avoiding preferential treatment of any of the inputs.

The tuning parameter α controls how quickly the magnitude of the weights decrease in the direction of the tail nodes and is empirically seen to control how ‘variable’ the sampled function is. If $\alpha > 1$ we refer to the prior as *trace-class*, coining the term *trace-class neural network priors*. If one believes that potentially many nodes with large weights are needed, one should choose α close to 1. See Figure 3 for three representative draws from the neural network prior. As the next theorem will show, this allows indeed to define an infinitely wide network by taking $N^{(l)} = \infty$, and the variances can be summarised in a diagonal covariance operator \mathcal{C} ; this prior is well-defined on an infinite-dimensional Hilbert space (isometric to ℓ^2), and can thus be used in the algorithms from Section 2. In practice, one truncates the

number of nodes within each layer as for the priors described before, or one may randomly switch nodes on and off similarly to the random truncation prior used in [9].

We now define the infinite width limit of the network. Given an infinite sequence of weights and biases for the first layer, distributed according to the prior (13), i.e. $\left\{ \left(B_i^{(1)}, W_{i,1}^{(1)}, \dots, W_{i,d}^{(1)} \right) : i \in \mathbb{N} \right\}$, all the functions of the first layer, $\{f_i^{(1)} : i \in \mathbb{N}\}$, are clearly well defined. We define all the functions of the second layer corresponding to an infinite-width first layer to be the following almost sure limits, assuming they exist:

$$(14) \quad F_i^{(2)}(x) = \lim_{N^1 \rightarrow \infty} B_i^{(2)} + \sum_{j=1}^{N^1} W_{i,j}^{(2)} \zeta(f_j^{(1)}(x)).$$

Assuming the random functions $\{F_i^{(2)} : i \in \mathbb{N}\}$ are well defined, proceeding iteratively, all the functions $\{F_i^{(l)} : i \in \mathbb{N}\}$ of subsequent layers, $l = 3, \dots, n$ and the output layer $F_1^{(n+1)}$ can be defined similarly. The functions in each layer of a finite width network are denoted with lower case to clearly distinguish them from their infinite width versions. For the output layer, the finite network gives $v(x)$ or $f_{n+1}^{(1)}(x)$ while the infinite network gives $V(x)$ or $F_{n+1}^{(1)}(x)$. In what follows, we will often write $v(x) = v_\theta(x)$ to emphasise the dependence of the function samples on the weights and biases. In order to simplify the presentation of the main results, we list a set of properties which will be shown to hold for our BNN prior:

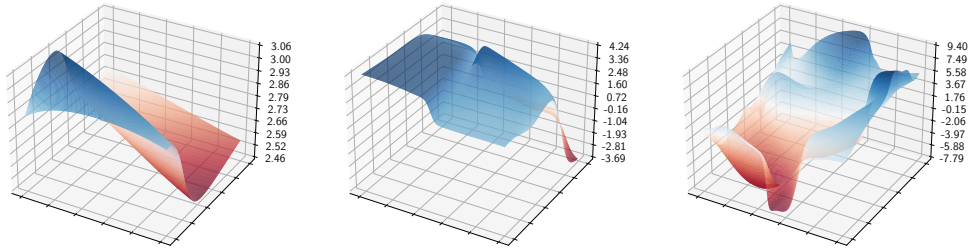


FIGURE 3. Three samples from the trace-class neural network prior defined on $[0, 1]^2$, for a network with 3 fully-connected layers and tanh activation functions; Tuning parameters are set to $\alpha = 1.5$, $\sigma_{w^{(l)}}^2 = \sigma_{b^{(l)}}^2 = 3$ for all $l = 1 \dots n + 1$ (left), $\alpha = 1.5$, $\sigma_{w^{(l)}}^2 = \sigma_{b^{(l)}}^2 = 30$ (centre), $\alpha = 1.0001$, $\sigma_{w^{(l)}}^2 = \sigma_{b^{(l)}}^2 = 30$ (right). The tuning parameter α controls the complexity of the prior functions, the variances in the layers control the overall variance. Note the difference in the magnitudes on the z -axis.

- (6) $\forall x \in [0, 1]^d$ one has $|f_i^{(l)}(x)| < \infty$ μ_0 -almost surely, $\mathbb{E} f_i^{(l)}(x) = 0$. Furthermore, there $\exists \sigma_l^2$ such that $\mathbb{E} \left[(f_i^{(l)}(x))^2 \right] < \sigma_l^2 / i^\alpha$ for all $x \in [0, 1]^d$. Here, both expectations are taken with respect to the prior on the parameters θ of the neural network. In particular this property holds for $v(x) = f_1^{(n+1)}(x)$.
- (7) $\exists c_l \geq 0$ such that $\forall x, y \in [0, 1]^d$, $\mathbb{E} \left[(f_i^{(l)}(x) - f_i^{(l)}(y))^2 \right] \leq c_l \|x - y\|^2 / i^\alpha$, with the expectation again taken with respect to the prior. In particular this gives $\mathbb{E} [v(x) - v(y)]^2 \leq c_{n+1} \|x - y\|^2$.

(8) μ_0 -almost surely, v is differentiable almost everywhere.

The first declared property ensures the output functions are appropriately finite in value and moments while the second property ensures a degree of smoothness. We now state a theorem which shows that the proposed prior satisfies the declared properties. To this end, we use an activation function² $\zeta : \mathbb{R} \rightarrow \mathbb{R}$ which satisfies the following condition, which will imply that $|\zeta(x)| < |x|$ for all $x \in \mathbb{R}$, and that ζ is differentiable almost everywhere, with the derivative being essentially bounded by 1:

(9) ζ is Lipschitz continuous with Lipschitz constant 1 and $\zeta(0) = 0$.³

Theorem 1. *Under Assumption 9, the functions of the layers of the finite-width neural network satisfy Properties 6, 7, and 8. In addition, if $\alpha > 1/2$, the functions on every layer of the infinite-width neural network (see (14)) exist almost surely and satisfy Properties 6 and 7, when the functions $f_i^{(l)}(x)$ and $v(x)$ therein are replaced with $F_i^{(l)}(x)$ and $V(x)$ defined as in (14). In addition, if the prior is trace-class (i.e. $\alpha > 1$), Property 1 is satisfied.*

The proof can be found in Appendix B.2.

3.1. Identifiability Issues and Remedies. It is well-known that the output function of a standard neural network does not depend on the labeling of functions within each layer. However, unlike a prior that has uniform variances within each layer, swapping nodes $f_i^{(l)}$ and $f_{i+1}^{(l)}$ (effectively by swapping their corresponding weights and biases) will lead from θ to a new θ' such that the prior weights change, and thus avoid the label-switching problem. To facilitate faster mixing by allowing jumps between these different configurations, we propose Algorithm 1, which can be found in Appendix A. The algorithm is well defined for finite widths networks, in which case the acceptance ratio is given by $a(\theta, \vartheta) = \mu_0(\vartheta)/\mu_0(\theta)$, but not for infinite width networks, see Lemma 6 in the Supplementary Material; this exemplifies the extra care needed when defining MCMC moves in the infinite dimension setting. One remedy is not to swap all the weights of the two selected nodes but only blocks of them, however we did not pursue this approach.

3.2. Illustrative Groundwater Flow Example. Before moving on to more challenging examples, we present an illustrative example, and compare the performance of the neural network prior to the Gaussian prior presented previously. The example, taken from [6]⁴, aims is to recover the permeability of an aquifer. The PDE $-\nabla \cdot (\exp(u(x))\nabla p(x)) = 0$ connects the log-permeability u of a porous medium to the hydraulic head function p with the boundary conditions given by (for $x = (x_1, x_2)$)

$$p(x) = x_1 \quad \text{if } x_2 = 0, \quad p(x) = 1 - x_1 \quad \text{if } x_2 = 1, \quad \frac{\partial p(x)}{\partial x_1} = 0 \quad \text{if } x_1 \in \{0, 1\}.$$

To enforce the permeability to be positive, the prior is defined for the log-permeability $u(x)$. We compare two priors. The first one is a trace-class neural network prior with 100 nodes, Tanh activation function, and a four dimensional input space with the inputs $(x_1, x_2, \sin(x_1), \sin(x_2))$. We set the tuning parameters to $\alpha = 1.001$, $\sigma_{w_1}^2 = \sigma_{b_1}^2 = 100$, $\sigma_{w_2}^2 = 1/30$, and $\sigma_{b_1}^2 = 1/10$. The second prior is a Gaussian measure on $[0, 1]^2$ with

²As will be clear from the proof of Theorem 1, one may use different activation functions at different layers, which will then all have to satisfy this assumption.

³The generalisation to arbitrary Lipschitz constants and the implication $\exists c > 0$ such that $\forall x \in \mathbb{R}$: $|\zeta(x)| < c|x|$ is straightforward.

⁴While we could not perfectly replicate their results, we aimed to stick as close to their results as possible.

the following orthonormal basis and corresponding eigenvalues defined using double indices $i = (i_1, i_2)$:

$$(15) \quad \varphi_i(x) = 2 \cos\left(\pi\left(i_1 + \frac{1}{2}\right)x_1\right) \cos\left(\pi\left(i_2 + \frac{1}{2}\right)x_2\right), \quad \lambda_i^2 = \frac{1}{(\pi^2((i_1 + 1/2)^2 + (i_2 + 1/2)^2))^{1.1}}.$$

In the experiments, we truncated the basis expansion using $1 \leq i_1, i_2 \leq 25$, which gives a similar number of parameters as we used in the neural network example. The true u^* is now defined using the same basis as $u^*(x) = \sum_i u_i^* \varphi_i(x)$ with $u_i^* = \lambda_i \sin((i_1 - 1/2)^2 + (i_2 - 1/2)^2) \cdot \delta[1 \leq i_1, i_2 \leq 10]$. The simulated data are 33 noisy observations of the true hydraulic head function p^* at various x positions, $y = p^*(x) + \varepsilon$, where $\varepsilon \sim \mathcal{N}(0, 0.01^2)$. The ‘true’ head function $p^*(x)$ is obtained by solving the forward PDE on a 40×40 grid. We ran pCN using both priors, and solving the forward problem on a 20×20 grid. Both experiments used a similar number of iterations and stored 1000 MCMC samples to obtain the mean estimates in Figure 4. The results in Figure 4 are less insightful and interpretable than those we will see in the next subsection as the few observations we have are related to the target function only through the PDE. A better comparison between, and validation of, the different priors is through visual posterior predictive checks as shown in Figure 5.

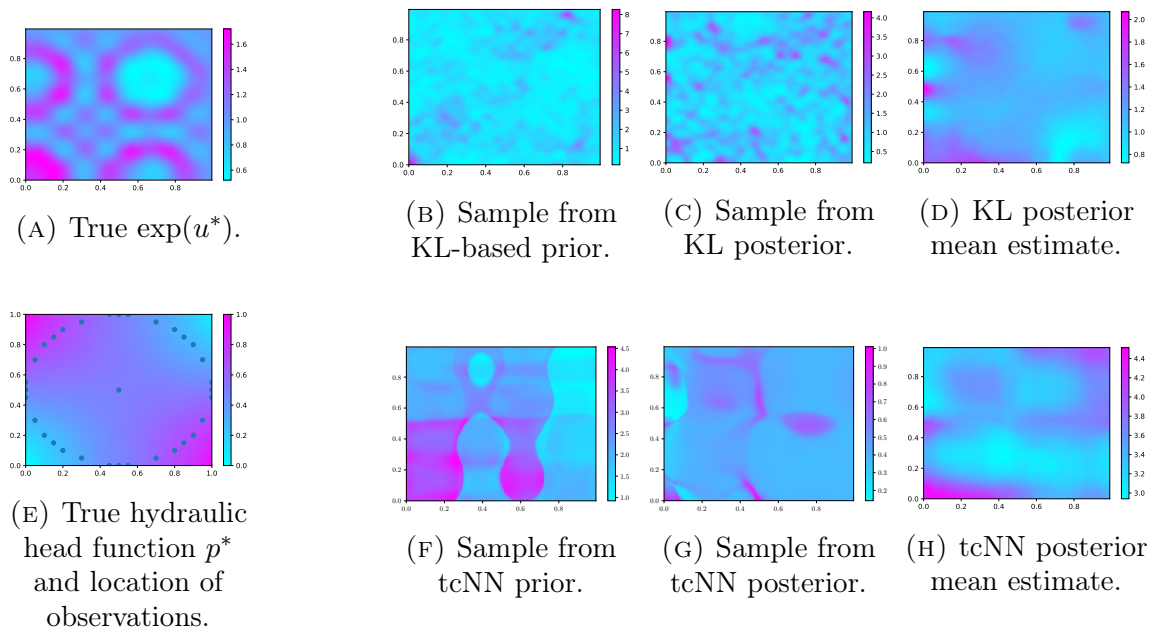


FIGURE 4. *Left column:* The true log-permeability (a), and its associated hydraulic head function (e) with the location of the 33 observations. *Top row, right columns:* A sample from the Gaussian prior (b), a sample from the associated posterior (c), and the posterior mean estimate obtained using pCN for the Gaussian prior (d). *Bottom row, right columns:* A sample from the trace-class neural network prior (f), a sample from the associated posterior (g), and the posterior mean estimate obtained using pCN for the neural network prior (h).

3.3. Ability to approximate complicated functions. To show that the trace-class neural network prior is able to visually recover relatively complicated functions, we define a

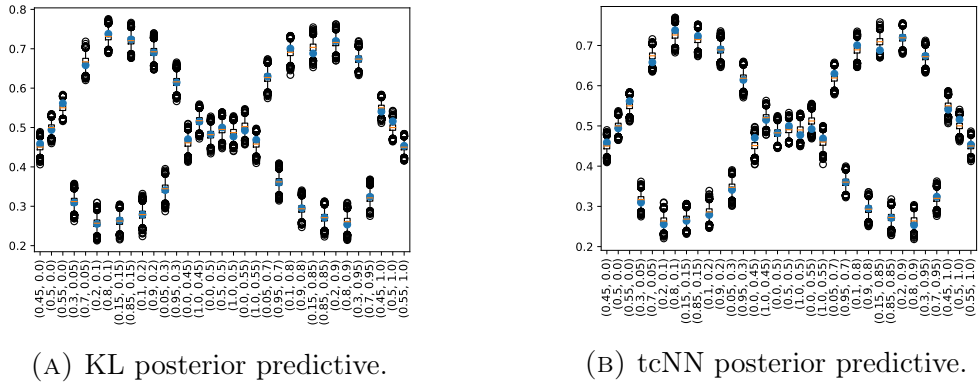


FIGURE 5. Visual posterior predictive check for both the KL- and tcNN-based posteriors. The observed values at each of the 33 observation locations (see figure 4) are shown as a blue dot, the box plots are 100 samples from the posterior predictive distribution [18, Section 6.3]. Both posteriors show similar predictive performance indicating that they arise from similarly well-suited priors.

function $u^* : [0, 1]^2 \rightarrow \mathbb{R}_+$, and observe this function on a 20×20 grid with independent Gaussian noise $\mathcal{N}(0, 0.01^2)$. The true u^* and the parameters of the prior we used here are the same one as in the example above. As Figure 6 shows, the neural network prior is able to approximate the true u^* when given many, in this example 400, observations.

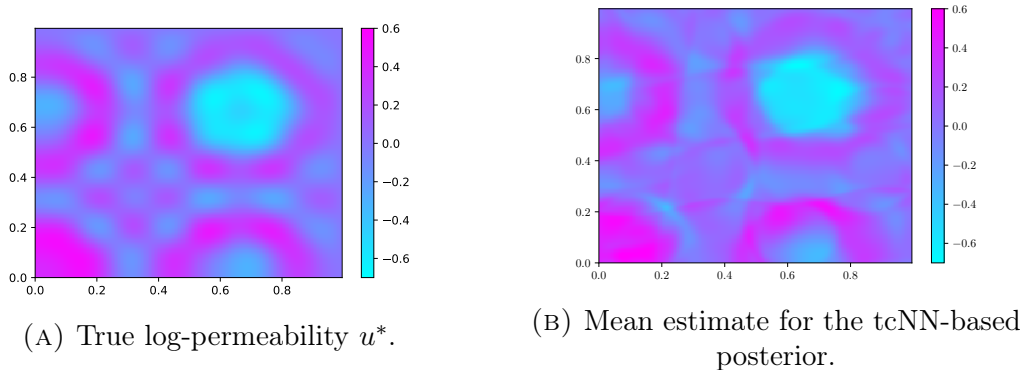


FIGURE 6. The neural network estimates the true $u^*(x)$ which is noisily observed on every grid point x of a 20×20 grid. In real applications, only few observations will be available, this example simply illustrates that many observations lead to close approximations for the trace-class neural network prior. Note that the functions displayed are shown on a fine grid, a coarse 20×20 sub-grid was used to generate the observations.

4. BAYESIAN LEARNING OF THE OPTIMAL VALUE FUNCTION

The solution to a stochastic optimal control problem is known as the *optimal value function* which can be found through Dynamic Programming (DP) (discussed in Section 4.1.) Reinforcement Learning is a popular and practical algorithmic approach for solving stochastic optimal control problems [47]. It finds the best control, which is a mapping from states to actions, in an online manner by using noisy estimates of the mathematical expectations to be maximised in DP. Online here refers to the use of the current best learnt control to

actuate the system to its next state which is also accompanied by a corresponding stochastic reward. This interaction with the system yields a stochastic process of actions, states and rewards with which DP’s mathematical expectations are estimated.

Automating a task can be made easier through the use of expert demonstrations, an approach known as Inverse Reinforcement Learning; see e.g. [39] for more nuanced details. Given the observed state, actions and rewards from an expert, we can exploit the mathematical formalism of Markov Decision Processes to relate this “data” to the optimal value function of the expert. In a Bayesian approach to this problem, one defines a prior on a function space that includes all admissible value functions. The data observed from the expert’s behaviour can then be used through a suitably defined likelihood [39] to infer the expert’s value function: having the expert’s value function at hand allows one to mimic their behaviour and hence defines an approach for automation. For discrete state spaces, [44] provide a method to quantify the uncertainty of the estimated value function. Here, we will generalise those ideas to continuous state spaces by using the priors introduced in the previous section.

4.1. Setup. A *Markov Decision Process* is defined by a controlled Markov chain $\{X_t\}_{t \in \mathbb{N}}$ called the *state process*, the *control process* $\{A_t\}_{t \in \mathbb{N}}$, and an optimality criterion. The state process takes values in a bounded set $\mathcal{X} \subset \mathbb{R}^d$, for simplicity we will assume the d -dimensional hypercube $\mathcal{X} = [0, 1]^d$. The control process is \mathcal{A} -valued, where $\mathcal{A} = \{1, \dots, M\}$ is a finite set. Given states $X_{1:t} = x_{1:t}$ and actions $A_{1:t} = a_{1:t}$ up to time t , the next state X_{t+1} is

$$(16) \quad X_{t+1} | (X_{1:t} = x_{1:t}, A_{1:t} = a_{1:t}) \sim p(\cdot | x_t, a_t),$$

where for any state-action pair (x_t, a_t) , $p(\cdot | x_t, a_t)$ is a probability density. In some applications, the state dynamics are deterministic, and thus there exists a map \mathcal{T} such that $X_{t+1} = \mathcal{T}(x_t, a_t)$. The action process depends on a *policy* $\mu : \mathcal{X} \rightarrow \mathcal{A}$ which is a deterministic mapping from the state space into the action space: $A_t | (X_{1:t} = x_{1:t}, A_{1:t-1} = a_{1:t-1}) \sim \delta_{\mu(x_t)}(\cdot)$. As there are many possible mappings $\mu : \mathcal{X} \mapsto \mathcal{A}$, we assume the agent executes a policy that is in some way optimal. To be more precise, let $r : \mathcal{X} \rightarrow \mathbb{R}$ be the *reward function*, then the *accumulated reward* given a policy μ and an initial state $X_1 = x_1$ is

$$C_\mu(x_1) = \mathbb{E}_\mu \left[\sum_{t=1}^{\infty} \beta^t r(X_t) | X_1 = x_1 \right],$$

where $\beta \in (0, 1)$ is a discount factor. The discount factor serves two purposes: it ensures that the expectation is well defined, and also that early actions are more important (in terms of the reward it adds to the total) than later ones, see [28] for a more detailed discussion. A policy μ^* is *optimal* if $C_{\mu^*}(x_1) \geq C_\mu(x_1)$ for all (μ, x_1) and the optimal policy can be found through the solution of Bellman’s fixed-point equation [3]. The function $v : \mathcal{X} \rightarrow \mathbb{R}$, which is the fixed-point solution to

$$v(x) = \max_{a \in \mathcal{A}} \left[r(x) + \beta \int_{\mathcal{X}} p(x' | x, a) v(x') dx' \right],$$

is called the *optimal value function* [4] and the corresponding optimal policy is

$$(17) \quad \mu^*(x) = \arg \max_{a \in \mathcal{A}} \left[\int_{\mathcal{X}} p(x' | x, a) v(x') dx' \right],$$

that is, the optimal action at any state is the one that maximises the expected value function at the next state.

4.2. Likelihood definition. The above decision making process gives optimal actions, but a human expert may occasionally pick non-optimal ones. To model imperfect action selections, noise is added to (17). At each time step the chosen action is a random variable given by

$$(18) \quad A_t(x_t) = \arg \max_{a \in \mathcal{A}} \left[\int_{\mathcal{X}} p(x'|x_t, a) v(x') dx' + \epsilon_t(a) \right],$$

where we assume $\epsilon_t \sim \mathcal{N}(0, \sigma^2 I_{M \times M})$ for some $\sigma > 0$. The Gaussian choice simplifies numerical calculations, and it is reasonable to assume that the variances for different actions are independent and identically distributed, but this assumption can be relaxed. From now on, we will assume that the state dynamics are deterministic, in which case the action selections occur according to

$$(19) \quad A_t(x_t) = \arg \max_{a \in \mathcal{A}} [v(\mathcal{T}(x_t, a)) + \epsilon_t(a)].$$

Our goal from now on will be to recover the optimal value function, and quantify the uncertainty thereof, by using the Hilbert space MCMC methods and the priors discussed in Sections 2 and 3.

The data consists of a collection of state-action pairs $y = \{y_t\}_{t=1}^T = \{(x_t, a_t)\}_{t=1}^T$ and the aim is to infer the value function (and thus the policy through (17)) that leads to the actions a_t for the current state x_t . Using the noisy action selection procedure (18), the likelihood is

$$(20) \quad \mathcal{L}(y|v, \sigma) = \prod_{t=1}^T p(a_t|x_t, v, \sigma) = \prod_{t=1}^T p(a_t|v_t, \sigma),$$

where the second equality follows by defining the vector v_t to contain the relevant evaluations of the value function to calculate the likelihood at y_t , i.e. using equation (19), the k -th entry of v_t is the evaluation of the value function $v(\cdot)$ at the location $\mathcal{T}(x_t, k)$, corresponding to starting at x_t and taking action $a = k \in \mathcal{A}$.

For a single observation $y_t = (x_t, a_t)$, we now drop the subscript t to simplify notation, and assume wlog that the optimal action is action $a = 1$, permuting the labels if necessary. The probability $p(a = 1|v, \sigma)$ (where v is a vector and $p(a|v, \sigma)$ is a probability mass function) can be computed using (18) by

$$(21) \quad p(a = 1|v, \sigma) = \int \mathbb{1}_{\{u \in \mathbb{R}^d: u_1 \geq u_j \forall j \neq 1\}} \mathcal{N}(u; v, \sigma^2 I_{M \times M}) du.$$

To compute this probability, we make use of the fact that the value of the integral is the same as the probability $\mathbb{P}(U_1 > U_j, \forall j \neq 1)$, where $U_k \sim \mathcal{N}(v(\mathcal{T}(x, k)), \sigma^2)$. This can be computed numerically using the pdf $\phi_1(\cdot)$ of U_1 and cdfs $\Phi_j(\cdot)$ of the remaining random variables U_j :

$$(22) \quad p(a = 1|v, \sigma) = \int_{-\infty}^{\infty} \phi_1(t) \Phi_2(t) \dots \Phi_M(t) dt = \frac{1}{\sigma} \int_{-\infty}^{\infty} \phi\left(\frac{t - v_1}{\sigma}\right) \prod_{j=2}^M \Phi\left(\frac{t - v_j}{\sigma}\right) dt.$$

where v_j is $v(\mathcal{T}(x, j))$. If the noise in (18) is not diagonal, this simplification cannot be made, and the integral (21) is harder to compute. More advanced numerical methods exist to efficiently calculate such integrals using Monte-Carlo simulations [19].

4.3. Likelihood gradient. Following from (22) we can compute the gradient of the likelihood in a data point (x_t, a_t) with respect to v_t . We again assume wlog that $a_t = 1 \in \mathcal{A}$ (by swapping the label of the first and the best action if necessary), and drop the subscript t ,

emphasising that v_k is the k -th entry of the vector $v = (v(\mathcal{T}(x, 1)), \dots, v(\mathcal{T}(x, M)))$. The partial derivatives with respect to the v_k are given by

(23)

$$\frac{\partial}{\partial v_1} p(a = 1|v, \sigma) = \frac{1}{\sigma} \int_{-\infty}^{\infty} \frac{t - v_1}{\sigma^2} \phi\left(\frac{t - v_1}{\sigma}\right) \prod_{j=2}^M \Phi\left(\frac{t - v_j}{\sigma}\right) dt$$

(24)

$$\frac{\partial}{\partial v_k} p(a = 1|v, \sigma) = -\frac{1}{\sigma^2} \int_{-\infty}^{\infty} \phi\left(\frac{t - v_1}{\sigma}\right) \phi\left(\frac{t - v_k}{\sigma}\right) \prod_{j=2, j \neq k}^M \Phi\left(\frac{t - v_j}{\sigma}\right) dt \quad k = 2 \dots M$$

(25)

$$= -\frac{1}{\sigma^2} \phi\left(\frac{v_1 - v_k}{\sqrt{2}\sigma}\right) \int_{-\infty}^{\infty} \phi\left(\frac{t - \frac{v_k + v_1}{2}}{\frac{\sigma}{\sqrt{2}}}\right) \prod_{j=2, j \neq k}^M \Phi\left(\frac{t - v_j}{\sigma}\right) dt,$$

where the last identity follows from the product of two Gaussian pdfs. This allows us, when using the neural network prior, to compute the gradient of the log-likelihood with respect to the parameters of the neural network, θ , using backpropagation. We emphasise that the vector $v = v(\theta)$ depends on these parameters, justifying the calculation of the Jacobian $\mathcal{D}_\theta v$. Using the chain rule, we get

$$(26) \quad \nabla_\theta \log p(a = 1|v, \sigma) = \frac{\nabla_\theta p(a = 1|v, \sigma)}{p(a = 1|v, \sigma)} = \frac{(\mathcal{D}_\theta v)^T \nabla_v p(a = 1|v, \sigma)}{p(a = 1|v, \sigma)}.$$

To get the entire gradient of the log-likelihood, we simply need to sum over all data points:

(27)

$$\nabla_\theta \ell(y|v, \sigma) = \nabla_\theta \log \left(\prod_{t=1}^T p(a_t|v_t, \sigma) \right) = \nabla_\theta \sum_{t=1}^T \log p(a_t|v_t, \sigma) = \sum_{t=1}^T \nabla_\theta \log p(a_t|v_t, \sigma),$$

where we only need to keep in mind the permutation in the actions when using (26).

When calculating (26), we note that $1 \cdot \nabla_v p(a|v, \sigma) = 0$ by translation invariance of v : $\mathcal{L}(y|v, \sigma) = \mathcal{L}(y|v + c, \sigma)$ for any constant function c , i.e. $c(x) = c(x')$ for all $x, x' \in \mathcal{X}$. The integrals involved in the gradient are in practice calculated numerically, and the arising errors may accumulate and cause numerical instabilities. To avoid these, one can ensure that the mean of these gradients is 0 by using the following modification, which we observed to enhance the performance in practice:

$$(28) \quad (26) = \frac{\sum_{k=1}^M ((\mathcal{D}_\theta v)^T)_k \left(\frac{\partial}{\partial v_k} p(a = 1|v, \sigma) - \sum_{k=1}^M \frac{\partial}{\partial v_k} p(a = 1|v, \sigma) \right)}{p(a = 1|v, \sigma)}.$$

The following theorem justifies the use of this likelihood in the function space MCMC setting, see [51, Chapter 12] for a definition of reproducing kernel Hilbert spaces (RKHS):

Theorem 2. *The log-likelihood $\ell(y|v, \sigma) = \log \mathcal{L}(y|v, \sigma)$ defined in (20) satisfies Assumptions 3 and 4, if $v \in \mathcal{H} = L_{\mathcal{K}}^2$, where $L_{\mathcal{K}}^2$ is any RKHS defined on L^2 .*

The proof can be found in Appendix B.4. We also note that when using the trace-class neural network prior from Section 3, the statements remain true if the likelihood is seen as a function of the parameters θ of the neural network:

Lemma 3. *The log-likelihood $\ell(y|v_\theta, \sigma)$ defined in (20) satisfies Assumptions 3 and 4, where now inference is over the weights and biases, $\theta \in \mathcal{H} = \ell^2$.*

Proof. The proof can be found in Appendix B.5. □

We now prove under which conditions on the likelihood one may use the preconditioned Crank-Nicolson Langevin algorithm when using the trace-class neural network prior, which in particular requires the gradient-informed proposals to be in the Cameron-Martin space of the prior. We will then remark on how it applies to the noisy action selection likelihood (19). For Theorem 4 assume the log-likelihood $\ell(y|v, \sigma)$ of the mapping $x \rightarrow v(x) \in \mathbb{R}$ is of the form

$$(29) \quad \ell(y|v, \sigma) = \sum_{t=1}^T \ell(a_t, v(x_t^1), \dots, v(x_t^M))$$

for some function $\ell : \mathcal{A} \times \mathbb{R}^M \rightarrow \mathbb{R}$, where a data point $y_t = (a_t, x_t^1, \dots, x_t^M)$ is comprised of $a_t \in \mathcal{A}$ and M points in the domain of v , i.e. $x_t^i \in \mathcal{X}$. Note that such a likelihood clearly encompasses (20). In the theorem below, we further assume uniformly bounded partial derivatives of the log-likelihood w.r.t. $v(x_t^i)$ for any t and i . Even with this assumption, to verify the assertion of Theorem 4, we need to establish the behaviour of moments of $\partial v(x)/\partial W_{i,j}^{(l)}$ and $\partial v(x)/\partial B_i^{(i)}$ for all x , weights and biases; details can be found in its proof.

Theorem 4. *Consider the infinite-width neural network with the Gaussian prior given in (13) with $\alpha > 1$ for its weights and biases, abbreviated to $N(0, \mathcal{C})$, and the log-likelihood 29. Assume $\sup_{v_{1:M} \in \mathbb{R}^M} |\partial \ell(a, v_1, \dots, v_M)/\partial v_i| < \infty$ for all i and $a \in \mathcal{A}$. Then Condition (5) holds for the pCNL implementation (10) for sampling from the posterior, that is $N(\mathcal{CD}\ell(u), \mathcal{C}) \simeq N(0, \mathcal{C})$ for $u \sim N(0, \mathcal{C})$ almost surely.*

The proof can be found in Appendix B.6. The proposed stochastic control likelihood given in (19) does not satisfy the assumption of the theorem since the partial derivatives are unbounded. To circumvent this, we apply a saturation function s to $v(x_t^i)$, and employ (19) with $s(v(\mathcal{T}(x_t, a)))$ instead of $v(\mathcal{T}(x_t, a))$. Lastly, we note that a similar result to Theorem 4 can be shown for the Hilbert space L^2 .

5. NUMERICAL ILLUSTRATIONS

This section aims to validate the theory, and highlight the applicability of the proposed priors and methodology. In particular, Section 5.2 confirms that, empirically, as the layer width for the trace-class neural network prior grows, the acceptance probability does not go to 0, a property known as ‘stability under mesh-refinement’ or ‘dimension-independence’. Section 5.3 compares the proposed trace-class neural network (tcNN) prior to a standard BNN prior and a KL prior, it highlights that, unlike the KL prior, the tcNN is scalable to higher-dimensional domains; and Section 5.4 shows that the posteriors can learn and mimic policies, thus justifying the use of these priors in the reinforcement learning setup. The code is available at <https://github.com/TorbenSell/trace-class-neural-networks>.

Throughout we use the Fourier basis (5) as the series expansion of choice when using the KL based prior, as this proved to be a good choice for reinforcement learning problems [30]. As a tuning parameter for the corresponding eigenvalues we set $\alpha = 2$ in (6), forcing the samples to be very smooth which we found to be a sensible choice in the discussed control problems. For the tcNN prior we used fully connected layers with tanh activation functions, and set $\sigma_{b^{(l)}}^2 = \sigma_{w^{(l)}}^2 = 2$ and $\alpha = 1.5$ in all the experiments, this again results in smooth sample functions. For the standard BNN we used the same architecture and set $\alpha = 0$ to get a constant variance sequence, in Section 5.2 we set $\sigma_{b^{(l)}}^2 = \sigma_{w^{(l)}}^2 = 10/(3N^{(l-1)})$ to highlight the dependence on the layer-width, in Sections 5.3 and 5.4 we set $\sigma_{b^{(l)}}^2 = \sigma_{w^{(l)}}^2 = 1/3$.

5.1. Control Problems: Setup. We set the scene by briefly describing the setup of the control problems which we use in the experiments, a detailed description can be found in the Supplementary Material.

The first example is the popular mountain car problem. A car is to drive up a mountain slope to reach a flag, but needs to gain momentum first by driving up the opposite mountain slope, thus initially driving away from the goal; see the left panel of Figure 7 for an illustration. The state space is the two-dimensional domain $\mathcal{X} = [-1.2, 0.6] \times [-0.07, 0.07]$ describing the vehicle’s position and velocity, and the action space contains three possible actions: $\mathcal{A} = \{-1, 0, 1\}$, representing exerting a constant force to the left, no force, and exerting the same constant force to the right, respectively. The likelihood (22) arises from $T = 50$ observations of state-action pairs, the data generating process is described in the Supplementary Material. The noise level in the likelihood is set to $\sigma = 0.1$.

The second example is the HalfCheetah example from the MuJoCo library [49], where an agent controls a two-dimensional cheetah with the aim to ‘run’ as fast as possible. For this example, the state space \mathcal{X} is 17-dimensional and the action space contains 8 possible actions. The likelihood (22) arises from $T = 100$ observations, we again refer to the Supplementary Material for the data generating process, and set the noise level in the likelihood to $\sigma = 0.1$. The right panel of Figure 7 shows the HalfCheetah.

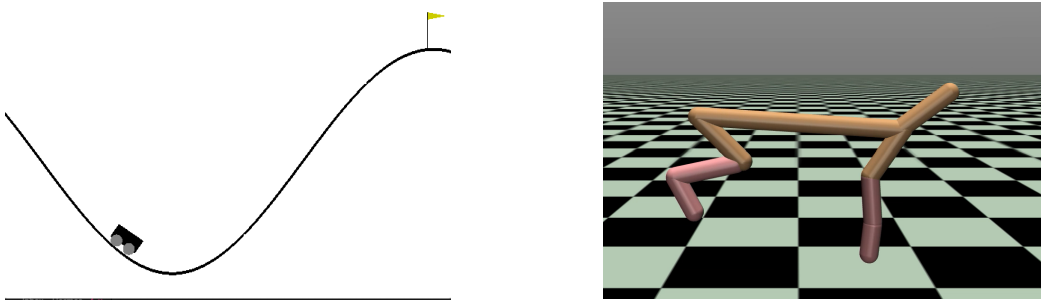


FIGURE 7. *Left:* The setup for the mountaincar example. The car’s goal is to reach the flag in as few steps as possible. The slope on the right is too steep to simply drive up the mountain, the car therefore has to gain momentum by going up the hill on the left first. *Right:* The HalfCheetah has states x_t in \mathbb{R}^{17} . Its goal is to run to the right as quickly as possible, while not moving its body parts more than necessary.

5.2. Dimension independence of trace-class neural network prior under mesh-refinement. We ran pCN for different network widths on the mountain car example. The network used has $l = 3$ hidden layers. As stated before, the tuning parameters in the prior are set to $\sigma_{b^{(l)}}^2 = \sigma_{w^{(l)}}^2 = 2$, and $\alpha = 1.5$. Table 1 displays the acceptance probability of pCN for a fixed step size when targeting the posteriors arising from the mountain car likelihood with a trace-class neural network prior and also a standard Bayesian neural network prior. The latter is characterised by setting $\alpha = 0$ in (13), resulting in a constant sequence of variances per layer. The other tuning parameters for the standard Bayesian neural network were set to $\sigma_{b^{(l)}}^2 = \sigma_{w^{(l)}}^2 = 10/(3N^{(l)})$. The step sizes chosen were $\beta = 1/10$ for the tcNN, $\beta = 1/7$ for the standard BNN.

5.3. Comparison of priors. To compare the trace-class neural network prior to the Karhunen-Loève prior, we used a large number of parameters for each, such that the error from truncating after finitely many nodes, or finitely many terms, is negligible. For both

$N^{(l)}$, for all l	10	20	30	40	50	60	70	80	90	100
Acc. ratio (tcNN)	22.8	24.0	23.5	22.1	22.2	23.1	23.9	23.4	23.0	23.9
Acc. ratio (BNN)	21.2	15.0	10.9	8.52	6.81	5.47	4.25	3.91	2.97	2.23
Total # of param.	261	921	1981	3441	5301	7561	10221	13281	16741	20601

TABLE 1. Acceptance ratios in % for both the trace-class neural network (tcNN) and standard Bayesian neural network (BNN) and total number of parameters (weights and biases) for different layer widths. 3 fully connected layers were used, and pCN was run over 3 hours for each choice of $N^{(l)}$. Notably the acceptance probability for the trace-class neural network proposed in this paper does not degenerate as more nodes are included per layer. Note that in the limit, only the tcNN is well-defined on the parameter space.

the mountaincar and the HalfCheetah example, we used the same trace-class neural network prior, with 3 hidden layers, and 100 nodes per layer, resulting in 20,601 parameters to be estimated for the mountaincar example, and 22,101 for the HalfCheetah example. For the Karhunen-Loève prior in the mountaincar example we set the truncation parameter to $k_{\max} = (70, 70)$ for (5) with eigenvalues (6) (recall that here $\alpha = 2$), resulting in a total of 19,880 coefficients to be estimated. For the KL prior in the HalfCheetah example we used approximation (3), and otherwise the same eigenfunctions and eigenvalues; due to the higher domain dimension $d = 17$, one would have to estimate 2,667,980 parameters. As this is too memory expensive for the computer used for the experiments, we used $k_{\max} = (10, 10)$ in the HalfCheetah example, resulting in 54,740 parameters to be estimated. Note that this increase in parameters to be estimated is despite the approximation (3) being used, and additionally truncating the expansions after fewer terms, highlighting the benefits of the dimension-robustness of the trace-class neural network prior.

To assess the quality of the priors, we ran pCN using 50 (for the mountaincar) and 100 (for the HalfCheetah) data points. For the mountain car example, we fixed five test points z_j , $j = 1, \dots, 5$ independent of the training data, and compared the posteriors by evaluating $v(z_j)$ at these new locations as estimated through MCMC runs. The top row in Figure 8 shows the resulting uncertainty estimates. As the value function is invariant under translations, we adjusted all samples such that they take the value 0 at the state which the optimal action a_{opt} takes one to:

$$(30) \quad v_{1:M}^{\text{centered}} = v_{1:M} - v_{a_{opt}} \cdot \mathbf{1},$$

where $\mathbf{1}$ denotes a vector of ones. For the HalfCheetah example, we looked at one test point for illustration, see the bottom row in Figure 8, and summarised the performance on another 100 test points (independent of the training data) in the Table 2, where we compared how the respective samples from the posterior do, as well as how the mean of all samples from the posterior in Section 5.4 (with a smaller number of nodes for the tcNN prior, and fewer active terms in the KL prior⁵) does on predicting the correct action (last two columns). Not surprisingly, the mean function is better at picking the correct action. Details on the data generating mechanism can be found in the Supplementary Material.

5.4. Ability to Learn Policy. To assess if the posteriors can truly learn an agent’s behaviour, we used the priors with a smaller number of parameters, and stored 1000 samples

⁵To calculate the mean function it is necessary to store the samples which (due to their used computer’s limited memory capacity) would not be feasible for the very wide layer prior, nor all the terms in the KL prior.

Decision by	KL samples	BNN samples	tcNN samples	KL mean	BNN mean	tcNN mean
Optimal	20.1%	18.1%	32.1%	25%	20%	42%
Non-optimal	79.9%	81.9%	67.9%	75%	80%	58%

TABLE 2. Actions picked using Equation 18 with v a posterior sample or the estimated posterior mean. The trace-class neural network prior outperforms the approximate KL and the standard BNN prior. The optimal action is computed using the same policy used to simulate data, see Section 5.1, the test points chosen at random from a representative episode of a HalfCheetah run. A random prediction would result in a success rate of 12.5%.

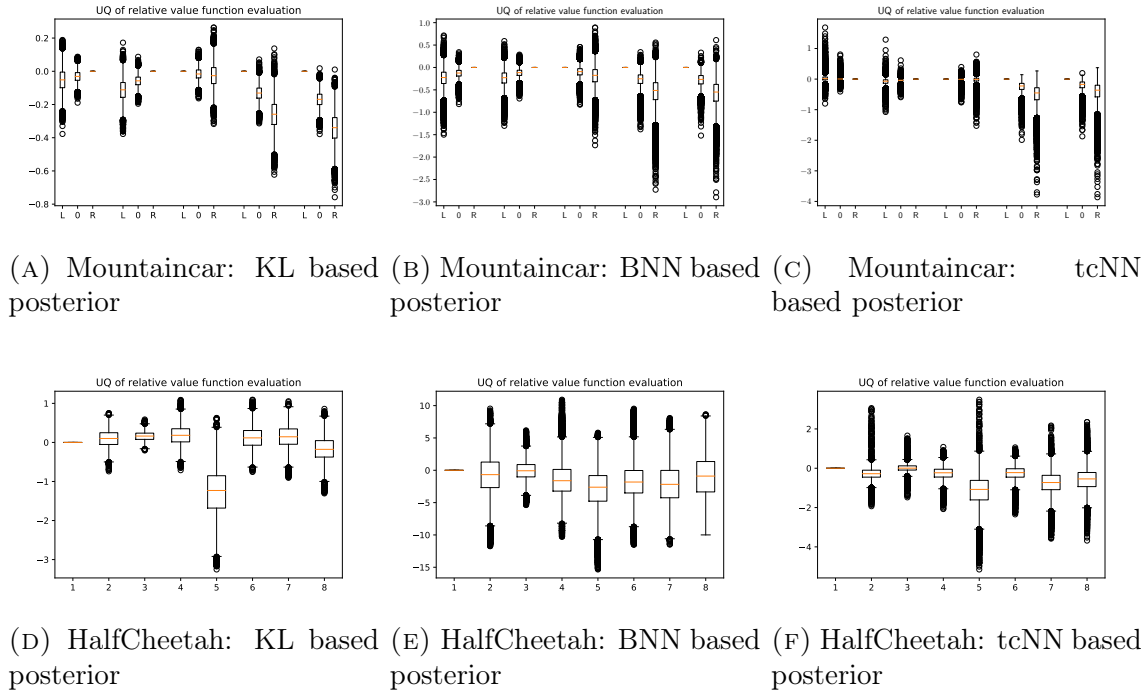


FIGURE 8. Uncertainty quantified using estimates arising from the three different priors for the mountaincar and the HalfCheetah examples.

Top row: Mountaincar example. In each plot, five different states are looked at, the estimates of the value functions are shown, standardised such that the optimal action has value 0 always using (30). None of the posteriors can make a clear judgement as to what the optimal actions for the first three shown states are, as the boxplots illustrate the uncertainty when predicting the best action. For the fourth and fifth states, all posteriors suggest a clear decision for action ‘Left’ as $v(\mathcal{T}(x, \text{‘Left’})) \gg v(\mathcal{T}(x, \text{‘0’})) \vee v(\mathcal{T}(x, \text{‘Right’}))$ cf. (19). The reader should note that the KL, the BNN, and the tcNN posteriors behave similarly in that they are uncertain in the first three states, and very decisive in the last two states.

Bottom row: HalfCheetah example. The optimal action is the first one in all three plots, and samples are again normalised using (30) such that they take the value 0 at the state the optimal value takes one to. The BNN and tcNN posteriors correctly estimate the optimal action, the KL posterior doesn’t.

for each posterior. We then used these samples to obtain a mean value function which was used for decision making. For the trace-class neural network prior we used 3 layers with 10 nodes per layer for both examples (resulting in 261 parameters for the mountaincar example and 411 for the HalfCheetah); for the KL prior we used $k_{\max} = (5, 5)$ for the mountaincar example (giving a total of 224 parameters), and $k_{\max} = (5, 5)$ in the HalfCheetah example (a total of 8,730 parameters). While the number of parameters can theoretically be chosen infinitely large, we truncated the layers and expansions earlier as we only had a very limited computational budget available. In general, where to truncate is an interesting model choice problem, and we found that for our problems the parameters described above yield very good approximations to a model with many more parameters. We thus chose to run the simplified model rather than a model with many more parameters, allowing many more stored MCMC posterior samples (1000 in this case) in the same wall-clock time. The results are summarised in Figure 9.

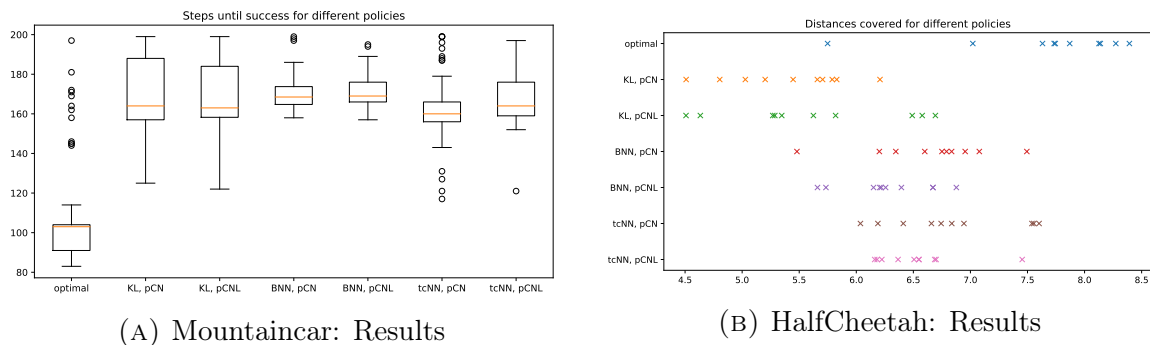


FIGURE 9. Results for the policy learning experiment.

Left: Mountaincar example. The number of steps until success is shown for different posteriors. If the goal was not reached after 200 steps, the run was counted as failure. Out of 100 runs, the policy following the KL posterior when using pCN gave 34 failures (24 when using pCNL), the standard BNN posterior gave 81 (pCN) and 80 (pCNL) failures, and the tcNN posteriors gave 23 (for the posterior estimates obtained using pCN) and 25 (pCNL).

Right: HalfCheetah example. The different policies arising from the KL posterior (obtained once using pCN, once using pCNL), a standard BNN posterior, and the tcNN posterior were controlling the agent over 10 runs with 100 time steps. The distances covered per run are shown in the plot.

6. CONCLUSION AND OUTLOOK

This paper addresses the problem of effective Bayesian inference for unknown functions with higher dimensional domains. Unlike priors which require an orthogonal basis for the function space and scale exponentially in the domain dimension, our proposed trace-class neural network prior easily scales to higher-dimensional domains as the dependence on the domain dimension is linear. When using the pCN sampling method, this prior also satisfies the desired property of being stable under mesh-refinement, in the sense that the acceptance probability of pCN does not degenerate to 0 when using more parameters for the neural network. Various questions remain unanswered though, and interesting directions for future work open up. For example, what are suitable generalisations of the proposed prior, e.g. heavy-tailed or hierarchical ones? What are the optimal settings for the tuning parameters $\sigma_w^{2(l)}$, $\sigma_b^{2(l)}$ and α ? Can one obtain contraction rates to ensure the concentration of the

posterior samples around the true functions? A first idea here is to exploit the various generalisations of the universal approximation theorem [43], and combine them with the proof methodology used in this paper.

We further introduced a likelihood suitable for Bayesian reinforcement learning where the underlying Markov decision process has a continuous state-space, and thus the unknown value function to be estimated has domain \mathbb{R}^d as opposed to a discrete set. An interesting research direction is to generalise this to continuous action spaces as well. Finally, we underscored the theory with numerical illustrations, illustrating the applicability of the prior for various control problems. It would also be interesting to evaluate the tcNN prior in other applied settings beyond control.

ACKNOWLEDGEMENTS

Part of this research was carried out when TS received financial support from the Cantab Capital Institute for the Mathematics of Information, he is currently supported by the EPSRC New Investigator award EP/V002694/1.

REFERENCES

- [1] Sergios Agapiou, Stig Larsson, and Andrew M Stuart. Posterior contraction rates for the bayesian approach to linear ill-posed inverse problems. *Stochastic Processes and Their Applications*, 123(10):3828–3860, 2013.
- [2] Sergios Agapiou, Masoumeh Dashti, and Tapio Helin. Rates of contraction of posterior distributions based on p-exponential priors. *Bernoulli*, 27(3):1616–1642, 2021.
- [3] Richard Bellman. On the theory of dynamic programming. *Proceedings of the National Academy of Sciences of the United States of America*, 38(8):716, 1952.
- [4] Dimitri P Bertsekas. *Dynamic Programming and Optimal Control*, volume 1. Athena scientific Belmont, MA, 1995.
- [5] Alexandros Beskos, Gareth Roberts, Andrew Stuart, and Jochen Voss. Mcmc methods for diffusion bridges. *Stochastics and Dynamics*, 8(03):319–350, 2008.
- [6] Alexandros Beskos, Mark Girolami, Shiwei Lan, Patrick E Farrell, and Andrew M Stuart. Geometric mcmc for infinite-dimensional inverse problems. *Journal of Computational Physics*, 335:327–351, 2017.
- [7] Greg Brockman, Vicki Cheung, Ludwig Pettersson, Jonas Schneider, John Schulman, Jie Tang, and Wojciech Zaremba. Openai gym, 2016.
- [8] Steve Brooks, Andrew Gelman, Galin Jones, and Xiao-Li Meng. *Handbook of Markov Chain Monte Carlo*. CRC press, 2011.
- [9] Simon L Cotter, Gareth O Roberts, Andrew M Stuart, and David White. Mcmc methods for functions: Modifying old algorithms to make them faster. *Statistical Science*, pages 424–446, 2013.
- [10] Tiangang Cui, Kody JH Law, and Youssef M Marzouk. Dimension-independent likelihood-informed mcmc. *Journal of Computational Physics*, 304:109–137, 2016.
- [11] Giuseppe Da Prato and Jerzy Zabczyk. *Stochastic Equations in Infinite Dimensions*. Cambridge university press, 2014.
- [12] Andreas Damianou and Neil Lawrence. Deep gaussian processes. In *Artificial Intelligence and Statistics*, pages 207–215, 2013.
- [13] Masoumeh Dashti, Stephen Harris, and Andrew Stuart. Besov priors for bayesian inverse problems. *arXiv preprint arXiv:1105.0889*, 2011.
- [14] Masoumeh Dashti, Kody JH Law, Andrew M Stuart, and Jochen Voss. Map estimators and their consistency in bayesian nonparametric inverse problems. *Inverse Problems*, 29(9):095017, 2013.

- [15] Matthew M Dunlop, Mark A Girolami, Andrew M Stuart, and Aretha L Teckentrup. How deep are deep gaussian processes? *The Journal of Machine Learning Research*, 19(1):2100–2145, 2018.
- [16] Andreas Eberle et al. Error bounds for metropolis–hastings algorithms applied to perturbations of gaussian measures in high dimensions. *The Annals of Applied Probability*, 24(1):337–377, 2014.
- [17] Herbert Federer. “geometric measure theory”, springer-verlag, berlin. *Heidelberg, New York*, 1969.
- [18] Andrew Gelman, John B Carlin, Hal S Stern, David B Dunson, Aki Vehtari, and Donald B Rubin. *Bayesian Data Analysis*. CRC press, 2013.
- [19] Alan Genz. Numerical computation of multivariate normal probabilities. *Journal of computational and graphical statistics*, 1(2):141–149, 1992.
- [20] Evarist Giné and Richard Nickl. *Mathematical Foundations of Infinite-dimensional Statistical Models*, volume 40. Cambridge University Press, 2016.
- [21] Martin Hairer, Andrew M Stuart, Sebastian J Vollmer, et al. Spectral gaps for a metropolis–hastings algorithm in infinite dimensions. *The Annals of Applied Probability*, 24(6):2455–2490, 2014.
- [22] W Keith Hastings. Monte carlo sampling methods using markov chains and their applications. 1970.
- [23] Kurt Hornik. Approximation capabilities of multilayer feedforward networks. *Neural networks*, 4(2):251–257, 1991.
- [24] Bamdad Hosseini. Well-posed bayesian inverse problems with infinitely divisible and heavy-tailed prior measures. *SIAM/ASA Journal on Uncertainty Quantification*, 5(1):1024–1060, 2017.
- [25] Bamdad Hosseini and Nilima Nigam. Well-posed bayesian inverse problems: Priors with exponential tails. *SIAM/ASA Journal on Uncertainty Quantification*, 5(1):436–465, 2017.
- [26] Marco A Iglesias, Kody JH Law, and Andrew M Stuart. Evaluation of gaussian approximations for data assimilation in reservoir models. *Computational Geosciences*, 17(5):851–885, 2013.
- [27] Arieh Iserles and Syvert P Nørsett. From high oscillation to rapid approximation iii: Multivariate expansions. *IMA journal of numerical analysis*, 29(4):882–916, 2009.
- [28] Leslie Pack Kaelbling, Michael L Littman, and Andrew W Moore. Reinforcement learning: A survey. *Journal of artificial intelligence research*, 4:237–285, 1996.
- [29] Bartek T Knapik, Aad W Van Der Vaart, J Harry van Zanten, et al. Bayesian inverse problems with gaussian priors. *The Annals of Statistics*, 39(5):2626–2657, 2011.
- [30] George Konidaris, Sarah Osentoski, and Philip Thomas. Value function approximation in reinforcement learning using the fourier basis. In *Twenty-fifth AAAI conference on artificial intelligence*, 2011.
- [31] Benedict Leimkuhler, Charles Matthews, and Tiffany Vlaar. Partitioned integrators for thermodynamic parameterization of neural networks. *arXiv preprint arXiv:1908.11843*, 2019.
- [32] Alexander G de G Matthews, Mark Rowland, Jiri Hron, Richard E Turner, and Zoubin Ghahramani. Gaussian process behaviour in wide deep neural networks. *arXiv preprint arXiv:1804.11271*, 2018.
- [33] Brent Minchew, Mark Simons, Scott Hensley, Helgi Björnsson, and Finnur Pálsson. Early melt season velocity fields of langjökull and hofsjökull, central iceland. *Journal of Glaciology*, 61(226):253–266, 2015.

- [34] Radford M Neal. *Bayesian Learning for Neural Networks*, volume 118. Springer Science & Business Media, 2012.
- [35] RM Neal. Bayesian learning for neural networks [phd thesis]. *Toronto, Ontario, Canada: Department of Computer Science, University of Toronto*, 1995.
- [36] RM Neal. Regression and classification using gaussian process priors. *Bayesian statistics*, 6:475, 1998.
- [37] Richard Nickl and Matteo Giordano. Consistency of bayesian inference with gaussian process priors in an elliptic inverse problem. *Inverse Problems*, 2020.
- [38] ALFIO Quarteroni, Andrea Manzoni, and Christian Vergara. The cardiovascular system: Mathematical modelling, numerical algorithms and clinical applications. *Acta Numerica*, 26:365–590, 2017.
- [39] Deepak Ramachandran and Eyal Amir. Bayesian inverse reinforcement learning. In *IJCAI*, volume 7, pages 2586–2591, 2007.
- [40] Gareth O Roberts and Jeffrey S Rosenthal. Optimal scaling of discrete approximations to langevin diffusions. *Journal of the Royal Statistical Society: Series B (Statistical Methodology)*, 60(1):255–268, 1998.
- [41] Gareth O Roberts, Richard L Tweedie, et al. Exponential convergence of langevin distributions and their discrete approximations. *Bernoulli*, 2(4):341–363, 1996.
- [42] Gareth O Roberts, Jeffrey S Rosenthal, et al. Optimal scaling for various metropolis–hastings algorithms. *Statistical science*, 16(4):351–367, 2001.
- [43] Franco Scarselli and Ah Chung Tsoi. Universal approximation using feedforward neural networks: A survey of some existing methods, and some new results. *Neural networks*, 11(1):15–37, 1998.
- [44] Sumeetpal S Singh, Nicolas Chopin, and Nick Whiteley. Bayesian learning of noisy markov decision processes. *ACM Transactions on Modeling and Computer Simulation (TOMACS)*, 23(1):4, 2013.
- [45] Ilya M Sobol. Sensitivity estimates for nonlinear mathematical models. *Mathematical modelling and computational experiments*, 1(4):407–414, 1993.
- [46] Andrew M Stuart. Inverse problems: A bayesian perspective. *Acta numerica*, 19:451–559, 2010.
- [47] Richard S Sutton and Andrew G Barto. *Reinforcement Learning: An Introduction*. MIT press, 2018.
- [48] Luke Tierney et al. A note on metropolis–hastings kernels for general state spaces. *The Annals of Applied Probability*, 8(1):1–9, 1998.
- [49] Emanuel Todorov, Tom Erez, and Yuval Tassa. Mujoco: A physics engine for model-based control. In *2012 IEEE/RSJ International Conference on Intelligent Robots and Systems*, pages 5026–5033. IEEE, 2012.
- [50] Aad W van der Vaart, J Harry van Zanten, et al. Rates of contraction of posterior distributions based on gaussian process priors. *The Annals of Statistics*, 36(3):1435–1463, 2008.
- [51] Martin J Wainwright. *High-dimensional statistics: A non-asymptotic viewpoint*, volume 48. Cambridge University Press, 2019.
- [52] Max Welling and Yee W Teh. Bayesian learning via stochastic gradient langevin dynamics. In *Proceedings of the 28th international conference on machine learning (ICML-11)*, pages 681–688, 2011.
- [53] Florian Wenzel, Kevin Roth, Bastiaan S Veeling, Jakub Świątkowski, Linh Tran, Stephan Mandt, Jasper Snoek, Tim Salimans, Rodolphe Jenatton, and Sebastian Nowozin. How good is the bayes posterior in deep neural networks really? *arXiv preprint arXiv:2002.02405*, 2020.

- [54] Przemyslaw Wojtaszczyk. *A Mathematical Introduction to Wavelets*, volume 37. Cambridge University Press, 1997.
- [55] Zhiqing Xiao. *Reinforcement Learning: Theory and Python Implementation*. China Machine Press, 2019.

APPENDIX A. NODESWAP ALGORITHM

Algorithm 1

```

1: procedure NODESWAP( $\theta$ )                                ▷ Input current iterate  $\theta$ 
2:    $\theta' \leftarrow \theta$                                 ▷ Priming the return value
3:    $l \sim \text{Unif}(n)$                                      ▷ Sample random layer
4:    $i \sim \text{Geom}(\alpha^{-1})$                              ▷ Sample random node
5:   while  $i \geq N_l$  do                                  ▷ Repeat process until we have a valid node index
6:      $i \sim \text{Geom}(\alpha^{-1})$ 
7:   end while
8:    $\forall j : w_{i+1,j}^{(l)'} \leftarrow w_{i,j}^{(l)}$ 
9:    $\forall j : w_{i,j}^{(l)'} \leftarrow w_{i+1,j}^{(l)}$ 
10:   $\forall j : w_{j,i+1}^{(l+1)'} \leftarrow w_{j,i}^{(l+1)}$ 
11:   $\forall j : w_{j,i}^{(l+1)'} \leftarrow w_{j,i+1}^{(l+1)}$ 
12:   $b_{i+1}^{(l)'} \leftarrow b_i^{(l)}$ 
13:   $b_i^{(l)'} \leftarrow b_{i+1}^{(l)}$ 
14:   $u \sim \text{Unif}([0, 1])$ 
15:   $a = \min(1, \mu_0(\theta')/\mu_0(\theta))$                     ▷ Metropolis-Hastings acceptance probability cf. (56)
16:  if  $u < a$  then
17:    return  $\theta'$                                        ▷ Accept node swap
18:  else
19:    return  $\theta$                                        ▷ Reject node swap
20:  end if
21: end procedure

```

APPENDIX B. PROOFS

Before turning to the proofs of the lemmas and theorems from the main paper, consider the n -layer fully connected feed-forward neural network in (12). When the layers have infinite width, we delineate the domain of the sequences that define each layer separately. For layer $1 < l < n + 1$ let

$$(31) \quad \mathcal{H}_w^{(l)} = \left\{ (w_{i,j}^{(l)})_{i,j \in \mathbb{N}} : \sum_{i=1}^{\infty} \sum_{j=1}^{\infty} (w_{i,j}^{(l)})^2 < \infty \right\}, \quad \mathcal{H}_b^{(l)} = \left\{ (b_i^{(l)})_{i \in \mathbb{N}} : \sum_{i=1}^{\infty} (b_i^{(l)})^2 < \infty \right\}.$$

(We omit the obvious modification for the sequence spaces for layer 1 and $n + 1$.) The entire network is then parameterised by

$$(32) \quad \mathcal{H} = \mathcal{H}^{(1)} \times \dots \times \mathcal{H}^{(n+1)}, \quad \text{where } \mathcal{H}^{(l)} = \mathcal{H}_w^{(l)} \times \mathcal{H}_b^{(l)}.$$

This domain is chosen because it has full measure under our Hilbert space Gaussian prior and also results in the infinite width functions in (14) being well defined almost surely.

B.1. Lemma 2.

Lemma 5. *Consider the n -layer fully connected feed-forward neural network in (12). When the layers have infinite width, their weights and biases can be equivalently parameterised by $\ell^2 = \{(a_1, a_2, \dots) \in \mathbb{R}^{\mathbb{N}} : \sum_i a_i^2 < \infty\}$.*

Proof. $\mathcal{H}_w^{(l)}$ in (31) is an instance of the Hilbert space ℓ^2 since $\mathbb{N} \times \mathbb{N}$ is countable and *any* enumeration (e.g. the ‘diagonal’ enumeration method) of $\mathcal{H}_w^{(l)}$ to map its elements to infinite sequences of the form (a_1, a_2, \dots) will be square summable. Similarly, $\mathcal{H}^{(l)} = \mathcal{H}_w^{(l)} \times \mathcal{H}_b^{(l)}$, the cartesian product of two ℓ^2 spaces is again an instance of ℓ^2 regardless of how the two sequences are merged into one. Finally, by the same arguments, $\mathcal{H} = \mathcal{H}^{(1)} \times \dots \times \mathcal{H}^{(n+1)}$ is also an instance of ℓ^2 . \square

B.2. Proof of Theorem 1.

Proof of Theorem 1. We prove the claims in the theorem for the infinite width case and in doing so cover the finite width case; the finite-dimensional case follows by omitting the limit arguments.

Lemma 5 shows that the weights and biases of the infinite width and finite depth neural network can be equivalently parameterised by ℓ^2 . As the biases and weights of each layer are independent zero mean Gaussian random variables, and the variances form a summable sequence when $\alpha > 1$, the prior μ_0 is a trace-class Gaussian prior on ℓ^2 and thus Property 1 is satisfied.

To see Property 6, by looking at the first layer we can easily check that for fixed $x \in [0, 1]^d$, $f_i^{(1)}(x)$ is a mixture of centered Gaussian distributions, and the claim follows by noting that $\mathbb{E}B_i^{(1)} = \mathbb{E}W_{i,j}^{(1)} = 0$,

$$\begin{aligned} \mathbb{E} \left[(f_i^{(1)}(x))^2 \right] &= \mathbb{E} \left[(B_i^{(1)})^2 \right] + \sum_{j=1}^d \mathbb{E} \left[(W_{i,j}^{(1)})^2 \right] (x_j)^2 \\ (33) \qquad \qquad \qquad &\leq \frac{\sigma_{b_1}^2}{i^\alpha} + \frac{\sigma_{w_1}^2}{i^\alpha} d \end{aligned}$$

$$(34) \qquad \qquad \qquad = \frac{1}{i^\alpha} [\sigma_{b_1}^2 + \sigma_{w_1}^2 d].$$

We use induction over l , and define the following random variables, for which we truncate the i -th function of layer l after k terms:

$$f_{i,k}^{(l)}(x) = B_i^{(l)} + \sum_{j=1}^k W_{i,j}^{(l)} \zeta(F_j^{(l-1)}(x)) \quad l = 2 \dots n + 1.$$

(Note that, with slight abuse of notation, we write $F_j^{(1)}$ even for the functions on the first layer, which are defined by finitely many parameters.)

By Assumption 9,

$$(35) \qquad \mathbb{E} \zeta(F_j^{(l-1)}(x)) \leq \mathbb{E} [|\zeta(F_j^{(l-1)}(x))|] \leq \mathbb{E} [|F_j^{(l-1)}(x)|] < \infty,$$

where the last inequality holds as $F_j^{(l-1)}(x)$ is L^2 bounded by the induction hypothesis.

We now show that $f_{i,k}^{(l)}(x) \rightarrow F_i^{(l)}(x)$ almost surely, and in L^2 , by applying the L^2 martingale convergence theorem. We thus need to show that $S_k(x) := f_{i,k}^{(l)}(x)$ is a L^2 bounded martingale, where we dropped the indices i and l for notational convenience. Indeed, with the natural filtration $(\mathcal{F}_k)_{k \in \mathbb{N}}$

$$\mathbb{E}[S_{k+1}(x) | \mathcal{F}_k] = 0,$$

as $W_{i,j}^{(l)}$ and $\zeta(F_j^{(l-1)}(x))$ are independent, the expectation of the former is centered, and the latter is finite. Additionally, by exploiting the independence, Assumption 9 and 35, we get

$$\begin{aligned}
(36) \quad \mathbb{E} [(S_k(x))^2] &= \mathbb{E}[B_i^{(l)}]^2 + \sum_{j=1}^k \mathbb{E} [(W_{i,j}^{(l)})^2] \mathbb{E} [(\zeta(F_j^{(l-1)}(x)))^2] \\
&\leq \frac{\sigma_{b^{(l)}}^2}{i^\alpha} + \sigma_{w^{(l)}}^2 \sum_{j=1}^k \frac{1}{(ij)^\alpha} \mathbb{E} [(F_j^{(l-1)}(x))^2] \leq \frac{\sigma_{b^{(l)}}^2}{i^\alpha} + \frac{\sigma_{w^{(l)}}^2 \sigma_{l-1}^2}{i^\alpha} \sum_{j=1}^k \frac{1}{j^{2\alpha}} \\
(37) \quad &= \frac{1}{i^\alpha} \left[\sigma_{b^{(l)}}^2 + \sigma_{w^{(l)}}^2 \sigma_{l-1}^2 \sum_{j=1}^k \frac{1}{j^{2\alpha}} \right].
\end{aligned}$$

This series converges for $\alpha > 1/2$, and we define the limit for $i = 1$ as σ_l^2 . Thus, S_k is indeed a L^2 bounded martingale and trivially $\mathbb{E} F_i^{(l)} = 0$, proving Assumption 6.

We next show Property 7. For the first layer, we use independence to get

$$\begin{aligned}
(38) \quad \mathbb{E} [(f_i^{(1)}(x) - f_i^{(1)}(y))^2] &= \sum_{j=1}^d \mathbb{E} [(W_{i,j}^{(1)})^2] (x_j - y_j)^2 \\
&= \frac{\sigma_{w_1}^2}{i^\alpha} \|x - y\|^2.
\end{aligned}$$

For the subsequent layers, we again use induction over l . We define $S_k(x)$ as before and check that

$$(39) \quad \mathbb{E} [(S_k(x)S_k(y))^2] = \mathbb{E} [(B_i^{(l)})^2] + \sum_{j=1}^k \mathbb{E} [(W_{i,j}^{(l)})^2] \mathbb{E} [\zeta(F_j^{(l-1)}(x))\zeta(F_j^{(l-1)}(y))].$$

Using the induction hypothesis, Assumption 9, (36) and (39) we get

$$\begin{aligned}
(40) \quad \mathbb{E} [(S_k(x) - S_k(y))^2] &= \mathbb{E} [(S_k(x))^2] + \mathbb{E} [(S_k(y))^2] - 2\mathbb{E}[S_k(x)S_k(y)] \\
&= 2\mathbb{E} [(B_i^{(l)})^2] + \sum_{j=1}^k \mathbb{E} [(W_{i,j}^{(l)})^2] \left(\mathbb{E} [\zeta(F_j^{(l-1)}(x))^2] + \mathbb{E} [\zeta(F_j^{(l-1)}(y))^2] \right) \\
&\quad - 2\mathbb{E}[S_k(x)S_k(y)] \\
&= \sigma_{w^{(l)}}^2 \sum_{j=1}^k \frac{1}{(ij)^\alpha} \mathbb{E} [(\zeta(F_j^{(l-1)}(x)) - \zeta(F_j^{(l-1)}(y)))^2] \\
&\leq \sigma_{w^{(l)}}^2 \sum_{j=1}^k \frac{1}{(ij)^\alpha} \mathbb{E} [(F_j^{(l-1)}(x) - F_j^{(l-1)}(y))^2] \\
&\leq \frac{\sigma_{w^{(l)}}^2 c_{l-1}}{i^\alpha} \|x - y\|^2 \sum_{j=1}^k \frac{1}{j^{2\alpha}}
\end{aligned}$$

$$(41) \quad = \frac{1}{i^\alpha} \left[\sigma_{w^{(l)}}^2 c_{l-1} \sum_{j=1}^k \frac{1}{j^{2\alpha}} \right] \|x - y\|^2,$$

such that the claim follows upon defining $c_l = \sigma_{w^{(l)}}^2 c_{l-1} \sum_{j=1}^{\infty} 1/j^{2\alpha}$, and noting that by the Fatou's lemma

$$\begin{aligned} \mathbb{E} \left[(F_i^{(l)}(x) - F_i^{(l)}(y))^2 \right] &= \mathbb{E} \left[\liminf_{k \rightarrow \infty} (S_k(x) - S_k(y))^2 \right] \\ &\leq \liminf_{k \rightarrow \infty} \mathbb{E} \left[(S_k(x) - S_k(y))^2 \right] \\ &\leq \liminf_{k \rightarrow \infty} \frac{1}{i^\alpha} \left[\sigma_{w^{(l)}}^2 c_{l-1} \sum_{j=1}^k \frac{1}{j^{2\alpha}} \right] \|x - y\|^2 \\ &= c_l \|x - y\|^2. \end{aligned}$$

Lastly, recall that by Assumption 9 the activation functions are Lipschitz continuous, and thus so is v as a composition of Lipschitz functions. The claim of Property 8 for the finite width case now follows since μ_0 -almost surely, v is Lipschitz continuous and thus differentiable almost everywhere by the Rademacher Theorem [17, Theorem 3.1.6]. \square

B.3. Lemma 6. In networks with small widths, Algorithm 1 gave acceptance rates of around 30% (for $N^{(l)} = 10$), which quickly declined as we included more nodes (e.g. 1% acceptances for $N^{(l)} = 100$.) This suggests that the NodeSwap algorithm is not well-defined in the infinite width limit, and this is indeed the statement of the next lemma. We will from now on write frakal letters for the swapped nodes $f_i^{(l)}$ and $f_{i+1}^{(l)}$, and reserve i and l for general indices.

Lemma 6. *The NodeSwap Algorithm 1 which swaps the biases and weights associated with the nodes $f_i^{(l)}$ and $f_{i+1}^{(l)}$ is not well defined in the infinite width limit.*

For the finite width network, the acceptance ratio is given by

$$(42) \quad a^N(\theta^N, \vartheta^N) = \frac{\mu_0^N(\vartheta^N)}{\mu_0^N(\theta^N)}.$$

Proof. By [48], one needs to check that the measures $\eta(d\theta, d\vartheta) := \mu(\theta)Q(\theta, d\vartheta)$ and $\eta^T(d\theta, d\vartheta) := \eta(d\vartheta, d\theta) = \mu(d\vartheta)Q(\vartheta, d\theta)$ are mutually absolutely continuous on a set $R \in (E \times E, \mathcal{E} \otimes \mathcal{E})$, and mutually singular on R^C , where here Q is the deterministic transition kernel, and (E, \mathcal{E}) is the measurable space on which μ and Q are defined.⁶ The (deterministic) transition kernel Q maps θ to ϑ by swapping the nodes $f_{ij}^{(l)}$ and $f_{i(j+1)}^{(l)}$ (or more precisely, their associated weights and biases) with probability

$$(43) \quad \frac{1}{n} \times \frac{1}{i^\alpha} \frac{1}{\sum_{j=1}^{N^l} \frac{1}{j^\alpha}},$$

which is well defined as $N^l \rightarrow \infty$, and independent of θ , such that it suffices to show that the measures $\mu(\theta)$ and $\mu^T(\theta) = \mu(\vartheta)$ are mutually absolutely continuous on a set $R_1 \in (E, \mathcal{E})$, and mutually singular on R_1^C . The likelihood is also invariant under the transformation $\theta \mapsto \vartheta$, and as it is integrable with respect to the prior by the assumptions in Section 2.2 [46], we only need to show that the Gaussian measures $\mu_0(d\theta)$ and $\mu_0^T(d\theta)$ are absolutely continuous with respect to one another. Note that we can write these as

$$(44) \quad \mu_0(d\theta) = \mathcal{N}(0, \mathcal{C})$$

$$(45) \quad \mu_0^T(d\theta) = \mathcal{N}(0, \tilde{\mathcal{C}}),$$

with diagonal (by assumption) covariance operators \mathcal{C} and $\tilde{\mathcal{C}}$, where the latter arises from swapping the variances associated with the swapped nodes. To see what is going on exactly,

⁶We use a different notation to [48]: Our η is his μ , our μ is his π , our (θ, ϑ) is his (x, y) .

we now change to the neural network notation, where the variances under \mathcal{C} for the individual weights and biases were given by

$$(46) \quad W_{i,j}^{(1)} \sim \mathcal{N}\left(0, \frac{\sigma_{w^{(1)}}^2}{i^\alpha}\right), \quad W_{i,j}^{(l)} \sim \mathcal{N}\left(0, \frac{\sigma_{w^{(l)}}^2}{(ij)^\alpha}\right) \text{ for } l = 2 \dots n+1, \quad B_i^{(l)} \sim \mathcal{N}\left(0, \frac{\sigma_{b^{(l)}}^2}{i^\alpha}\right).$$

The variances under $\tilde{\mathcal{C}}$ are the same for most weights and biases, changed are only those associated with the swap nodes (recall that we swap nodes $f_{ij}^{(l)}$ and $f_{i(i+1)}^{(l)}$). The only changed variances are

$$(47) \quad W_{i,j}^{(l)} \sim \mathcal{N}\left(0, \frac{\sigma_{w^{(l)}}^2}{((i+1)j)^\alpha}\right), \quad W_{(i+1),j}^{(l)} \sim \mathcal{N}\left(0, \frac{\sigma_{w^{(l)}}^2}{(ij)^\alpha}\right), \quad \forall j \in \mathbb{N}$$

$$(48) \quad W_{i,j}^{(l+1)} \sim \mathcal{N}\left(0, \frac{\sigma_{w^{(l+1)}}^2}{(i(j+1))^\alpha}\right), \quad W_{i(j+1)}^{(l+1)} \sim \mathcal{N}\left(0, \frac{\sigma_{w^{(l+1)}}^2}{(ij)^\alpha}\right), \quad \forall i \in \mathbb{N}$$

$$(49) \quad B_i^{(l)} \sim \mathcal{N}\left(0, \frac{\sigma_{b^{(l)}}^2}{(i+1)^\alpha}\right) \quad B_{i+1}^{(l)} \sim \mathcal{N}\left(0, \frac{\sigma_{b^{(l)}}^2}{i^\alpha}\right),$$

which corresponds to swapping all the weights going into the nodes, swapping all the weights leaving the nodes, and swapping the biases of the nodes, respectively (see Figure 2 for an illustration).

We apply the Feldman-Hajek Theorem [11, Theorem 2.25] to prove that these two Gaussian measures are mutually singular, by showing that the operator $(\mathcal{C}^{-1/2}\tilde{\mathcal{C}}^{1/2})(\mathcal{C}^{-1/2}\tilde{\mathcal{C}}^{1/2})^*$ is *not* a Hilbert-Schmidt operator. Due to the diagonality of \mathcal{C} and $\tilde{\mathcal{C}}$ the operator would be a Hilbert-Schmidt operator if

$$(50) \quad \sum_{i=1}^{\infty} \left(\frac{\tilde{\lambda}_i^2}{\lambda_i^2} - 1 \right)^2 < \infty.$$

We only need to check those terms where $\tilde{\lambda}_i \neq \lambda_i$. Again looking at only the eigenvalues corresponding to the weights going into the swapped nodes, and switching to the neural network parametrisation, we have

$$(51) \quad \sum_{j=1}^{\infty} \left(\frac{(ij)^\alpha}{((i+1)j)^\alpha} - 1 \right)^2 + \sum_{j=1}^{\infty} \left(\frac{((i+1)j)^\alpha}{(ij)^\alpha} - 1 \right)^2 = \infty,$$

such that the operator is *not* a Hilbert-Schmidt operator, and the Gaussian measures are mutually singular.

For the interested reader, note that the other two conditions of the Feldman-Hajek Theorem [11, Theorem 2.25] are satisfied. First we show only that there exist constants L and U such that for any $\theta \in \ell^2$,

$$(52) \quad L|\tilde{\mathcal{C}}\theta| \leq |\mathcal{C}\theta| \leq U|\tilde{\mathcal{C}}\theta|,$$

which is equivalent to

$$(53) \quad L \sum_{i=1}^{\infty} \left(\theta_i \tilde{\lambda}_i^2 \right)^2 \leq \sum_{i=1}^{\infty} \left(\theta_i \lambda_i^2 \right)^2 \leq U \sum_{i=1}^{\infty} \left(\theta_i \tilde{\lambda}_i^2 \right)^2,$$

where λ_i^2 are the respective variances corresponding to the values. Firstly note that we only need to consider those terms for which $\tilde{\lambda}_i^2 \neq \lambda_i^2$. Using the neural network parametrisation, we can split the problem in showing that (53) holds for A) all the weights going into the

swapped nodes, B) all the weights leaving the swapped nodes, and C) swapping the biases. Looking at the weights going into the swapped nodes, note that

$$\begin{aligned}
\sum_{j=1}^{\infty} \left(\frac{w_{ij}^{(l)}}{((i+1)j)^\alpha} \right)^2 + \sum_{j=1}^{\infty} \left(\frac{w_{(i+1)j}^{(l)}}{(ij)^\alpha} \right)^2 &= \sum_{j=1}^{\infty} \left(\frac{w_{ij}^{(l)}}{(ij)^\alpha} \right)^2 \left(\frac{(ij)^\alpha}{((i+1)j)^\alpha} \right)^2 \\
&\quad + \sum_{j=1}^{\infty} \left(\frac{w_{(i+1)j}^{(l)}}{((i+1)j)^\alpha} \right)^2 \left(\frac{((i+1)j)^\alpha}{(ij)^\alpha} \right)^2 \\
&\leq \sum_{j=1}^{\infty} \left(\frac{w_{ij}^{(l)}}{(ij)^\alpha} \right)^2 + 2^{2\alpha} \sum_{j=1}^{\infty} \left(\frac{w_{(i+1)j}^{(l)}}{((i+1)j)^\alpha} \right)^2 \\
&\leq 2^{2\alpha} \left[\sum_{j=1}^{\infty} \left(\frac{w_{ij}^{(l)}}{(ij)^\alpha} \right)^2 + \sum_{j=1}^{\infty} \left(\frac{w_{(i+1)j}^{(l)}}{((i+1)j)^\alpha} \right)^2 \right],
\end{aligned}$$

and

$$\begin{aligned}
\sum_{j=1}^{\infty} \left(\frac{w_{ij}^{(l)}}{(ij)^\alpha} \right)^2 + \sum_{j=1}^{\infty} \left(\frac{w_{(i+1)j}^{(l)}}{((i+1)j)^\alpha} \right)^2 &= \sum_{j=1}^{\infty} \left(\frac{w_{ij}^{(l)}}{((i+1)j)^\alpha} \right)^2 \left(\frac{((i+1)j)^\alpha}{(ij)^\alpha} \right)^2 \\
&\quad + \sum_{j=1}^{\infty} \left(\frac{w_{(i+1)j}^{(l)}}{(ij)^\alpha} \right)^2 \left(\frac{(ij)^\alpha}{((i+1)j)^\alpha} \right)^2 \\
&\leq 2^{2\alpha} \sum_{j=1}^{\infty} \left(\frac{w_{ij}^{(l)}}{((i+1)j)^\alpha} \right)^2 + \sum_{j=1}^{\infty} \left(\frac{w_{(i+1)j}^{(l)}}{(ij)^\alpha} \right)^2 \\
&\leq 2^{2\alpha} \left[\sum_{j=1}^{\infty} \left(\frac{w_{ij}^{(l)}}{((i+1)j)^\alpha} \right)^2 + \sum_{j=1}^{\infty} \left(\frac{w_{(i+1)j}^{(l)}}{(ij)^\alpha} \right)^2 \right]
\end{aligned}$$

such that for the weights going into the swapped nodes, (53) holds with $L = 2^{-2\alpha}$ and $U = 2^{2\alpha}$. Repeating the same argument for the weights leaving the swapped nodes and for the biases, shows that (53) holds in general with $L = 2^{-2\alpha}$ and $U = 2^{2\alpha}$. The remaining condition of the Feldman-Hajek theorem addresses the difference of means, but as $\theta = 0$ this is clearly in the Cameron-Martin space of the prior.

For the acceptance ratio in the finite width networks, observe that the likelihood does not depend on the labelling of the nodes and thus plays no role in the acceptance probability. Similarly, the transition kernel is symmetric, as nodes $f_i^{(l)}$ and $f_{i+1}^{(l)}$ are swapped with probability

(54)

$$\begin{aligned}
q^N(\vartheta^N | \theta^N) &= \mathbb{P}(\{\text{layer } l \text{ gets chosen}\}) \times \mathbb{P}(\{\text{node } i \text{ gets chosen}\} | \{\text{layer } l \text{ got chosen}\}) \\
(55) \quad &= \frac{1}{n+1} \times \frac{1}{i^\alpha} \frac{1}{\sum_{j=1}^{N^l} \frac{1}{j^\alpha}}.
\end{aligned}$$

For the finite dimensional case we thus get

$$(56) \quad a^N(\theta^N, \vartheta^N) = \frac{\mu_0^N(\vartheta^N)}{\mu_0^N(\theta^N)} \frac{\mathcal{L}^N(\vartheta^N)}{\mathcal{L}^N(\theta^N)} \frac{q^N(\theta^N | \vartheta^N)}{q^N(\vartheta^N | \theta^N)} = \frac{\mu_0^N(\vartheta^N)}{\mu_0^N(\theta^N)},$$

which is as required. \square

B.4. Proof of Theorem 2.

Proof of Theorem 2. For a given data point $y = (x, a)$, let the actions be enumerates such that $a = 1$. Let further $v = (v_1, \dots, v_M) := (v(\mathcal{T}(x, 1)), \dots, v(\mathcal{T}(x, M)))$ be the vector of the value function evaluations relevant for the likelihood computation. The integral (21) is trivially upper bounded by 1. Define $\bar{v} = \max_j |v_j|$. For the lower bound, we use (22) to get

$$\begin{aligned}
(21) &\geq \frac{1}{\sigma} \int_{-\infty}^{\infty} \phi\left(\frac{t-v_1}{\sigma}\right) \frac{1}{2^{M-1}} \prod_{j=2}^M \mathbb{1}_{\{\Phi((t-v_j)/\sigma) \geq 1/2\}} dt \\
&= \frac{1}{\sigma 2^{M-1}} \int_{-\infty}^{\infty} \phi\left(\frac{t-v_1}{\sigma}\right) \prod_{j=2}^M \mathbb{1}_{\{t \geq v_j\}} dt \\
&\geq \frac{1}{\sigma 2^{M-1}} \int_{-\infty}^{\infty} \phi\left(\frac{t-v_1}{\sigma}\right) \prod_{j=1}^M \mathbb{1}_{\{t \geq v_j\}} dt \\
&\geq \frac{1}{\sigma 2^{M-1}} \int_{\bar{v}}^{\infty} \phi\left(\frac{t-v_1}{\sigma}\right) dt \geq \frac{1}{\sigma 2^{M-1}} \int_{2\bar{v}}^{\infty} \phi\left(\frac{t}{\sigma}\right) dt \\
(57) \quad &\geq \frac{1}{\sigma 2^{M+1} \sqrt{2\pi\sigma^2\bar{v}}} \exp(-(4\bar{v}^2/(2\sigma^2))).
\end{aligned}$$

Since v is in a reproducing kernel Hilbert space \mathcal{H} , there exists for any $x \in \mathcal{X}$ a C_x such that $|v(x)| \leq C_x \|v\|_{\mathcal{H}}$ for all $v \in \mathcal{H}$ [51, Chapter 12], and taking $C = \max_{j \in \{1, \dots, M\}} C_{\mathcal{T}(x, j)}$, we have $\bar{v} \leq C \|v\|_{\mathcal{H}}$.

Taking logarithms of (57), we thus have

$$\begin{aligned}
(58) \quad \ell(y|v, \sigma) &\stackrel{(57)}{\geq} -\log(\sigma 2^M \sqrt{2\pi\sigma^2}) - \log(\bar{v}) - \frac{\bar{v}^2}{2\sigma^2} \\
&\geq -\log(\sigma 2^M \sqrt{2\pi\sigma^2}) - \left(1 + \frac{1}{2\sigma^2}\right) \cdot \bar{v}^2 \\
&\geq -\log(\sigma 2^M \sqrt{2\pi\sigma^2}) - C \cdot \left(1 + \frac{1}{2\sigma^2}\right) \cdot \|v\|_{\mathcal{H}}^2
\end{aligned}$$

showing that Assumption 3 holds with $K = \max\left\{\log(\sigma 2^M \sqrt{2\pi\sigma^2}), C \cdot \left(1 + \frac{1}{2\sigma^2}\right)\right\}$ and $p = 2$.

To see that Assumption 4 holds, assume that $\max\{\|u\|_{\mathcal{H}}, \|v\|_{\mathcal{H}}\} < r$. Then, since the log-likelihood is continuously differentiable in (v_1, \dots, v_M) , for any \bar{r} there exists a constant $C(\bar{r})$ such that for any vectors $u_{1:M}, v_{1:M}$ with $\max_j |u_j| \leq \bar{r}$, $\max_j |v_j| \leq \bar{r}$ one has by the mean value theorem that

$$(59) \quad |\ell(y|u, \sigma) - \ell(y|v, \sigma)| \leq C(\bar{r}) \cdot (|u_1 - v_1| + \dots + |u_M - v_M|).$$

Using the RKHS property as before, we note that $\bar{u} = \max_j |u_j| < \max_j C_{\mathcal{T}(x, j)} r$ and $\bar{v} = \max_j |v_j| < \max_j C_{\mathcal{T}(x, j)} r$. We also use the fact that for any $x \in \mathcal{X}$ there exists a C_x such that $|(u-v)(x)| \leq C_x \|u-v\|_{\mathcal{H}}$ for all $u, v \in \mathcal{H}$. Taking $\bar{r} = \max_j C_{\mathcal{T}(x, j)} r > 0$ we thus

get

$$\begin{aligned}
|\ell(y|u, \sigma) - \ell(y|v, \sigma)| &\stackrel{59}{\leq} C(\bar{r}) \cdot (|u_1 - v_1| + \cdots + |u_M - v_M|) \\
&= C(\bar{r}) \cdot (|(u - v)(\mathcal{T}(x, 1))| + \cdots + |(u - v)(\mathcal{T}(x, M))|) \\
&\leq C(\bar{r}) \cdot \sum_{j=1}^M C_{\mathcal{T}(x,j)} \cdot \|u - v\|_{\mathcal{H}},
\end{aligned}$$

such that the assumption holds with $K(r) = C(\bar{r}) \cdot \sum_{j=1}^M C_{\mathcal{T}(x,j)}$. \square

B.5. Proof of Lemma 3.

Proof of Lemma 3. Let $\theta = (w, b)$ be the collection of all weights and biases. Using the definition of the neural network (12), we let $\hat{x} = (1, x) \in \mathbb{R}^{d+1}$ and note that

$$|f_i^{(1)}(x)|^2 = |\langle (b_i^{(1)}, w_{i,:}^{(1)}), \hat{x} \rangle|^2 \leq \|\hat{x}\|_2^2 \cdot \|(b_i^{(1)}, w_{i,:}^{(1)})\|_2^2 \leq (1 + \|x\|_2^2) \cdot \|(b_i^{(1)}, w_{i,:}^{(1)})\|_2^2$$

by the Cauchy-Schwartz inequality (CSI). We now note that, regardless of the choice of $N^{(1)}$,

$$\|f_{1:N^{(1)}}^{(1)}(x)\|_2^2 = \sum_{i=1}^{N^{(1)}} |f_i^{(1)}(x)|^2 \leq (1 + \|x\|_2^2) \cdot \sum_{i=1}^{N^{(1)}} \|(b_i^{(1)}, w_{i,:}^{(1)})\|_2^2 \leq (1 + \|x\|_2^2) \cdot \|\theta\|_{\ell^2}^2,$$

such that the result holds also for the limit $N^{(1)} \rightarrow \infty$. For the higher layers, we use Assumption 9 and get for any l that $|\zeta(f_i^{(l)}(x))|^2 \leq |f_i^{(l)}(x)|^2$. We apply the CSI a few more times, and get that

$$\begin{aligned}
|f_i^{(l)}(x)|^2 &= |b_i^{(l)} + \sum_{j=1}^{N^{(l-1)}} w_{i,j}^{(l)} \zeta(f_j^{(l-1)}(x))|^2 \\
&\leq (1 + \|\zeta(f_{1:N^{(l-1)}}^{(l-1)}(x))\|_2^2) \cdot \|(b_i^{(l)}, w_{i,:}^{(l)})\|_2^2 \\
&\leq (1 + \|f_{1:N^{(l-1)}}^{(l-1)}(x)\|_2^2) \cdot \|(b_i^{(l)}, w_{i,:}^{(l)})\|_2^2,
\end{aligned}$$

and that

$$\begin{aligned}
\|f_{1:N^{(l)}}^{(l)}(x)\|_2^2 &= \sum_{i=1}^{N^{(l)}} |f_i^{(l)}(x)|^2 \leq (1 + \|\zeta(f_{1:N^{(l-1)}}^{(l-1)}(x))\|_2^2) \cdot \sum_{i=1}^{N^{(l)}} \|(b_i^{(l)}, w_{i,:}^{(l)})\|_2^2 \\
&\leq (1 + \|f_{1:N^{(l-1)}}^{(l-1)}(x)\|_2^2) \cdot \|\theta\|_{\ell^2}^2.
\end{aligned}$$

For any θ with $\|\theta\|_{\ell^2}^2 < 1$, we use induction and get that $|f_i^{(l)}(x)|^2 \leq l + \|x\|^2$. If $\|\theta\|_{\ell^2}^2 \geq 1$, we get again by induction that $|f_i^{(l)}(x)|^2 \leq (l + \|x\|^2) \cdot \|\theta\|_{\ell^2}^{2l}$; such that for any θ ,

$$(60) \quad \|f_{1:N^{(l)}}^{(l)}(x)\|_2^2 = \sum_{i=1}^{N^{(l)}} |f_i^{(l)}(x)|^2 \leq (l + \|x\|^2) \cdot (1 + \|\theta\|_{\ell^2}^{2l}),$$

in particular for $v(x) = f_1^{(n+1)}(x)$ we have

$$|v(x)|^2 \leq (n + 1 + \|x\|^2) \cdot (1 + \|\theta\|_{\ell^2}^{2(n+1)}).$$

Using the same bound for $\ell(y|v, \sigma)$ as in the proof of Theorem 2 given in (58), we get

$$\begin{aligned} \ell(y|v, \sigma) &\geq -\log(\sigma 2^M \sqrt{2\pi\sigma^2}) - \left(1 + \frac{1}{2\sigma^2}\right) \cdot \bar{v}^2 \\ &\geq -\log(\sigma 2^M \sqrt{2\pi\sigma^2}) - (n+1 + \max_j \|\mathcal{T}(x, j)\|^2) \cdot \left(1 + \frac{1}{2\sigma^2}\right) \cdot (1 + \|\theta\|_{\ell^2}^{2(n+1)}), \end{aligned}$$

such that the result holds with $K = (n+1 + \max_j \|\mathcal{T}(x, j)\|^2) \cdot (1 + \frac{1}{2\sigma^2}) + \max\{\|\theta\|, \|\tilde{\theta}\|\}$ and $p = 2(n+1)$. Note that the constant K is independent of the layer width and the result holds for networks of arbitrary width.

To prove Assumption 4, fix $r > 0$ and consider the sequences $\theta, \tilde{\theta} \in \ell^2$ such that $\max\{\|\theta\|, \|\tilde{\theta}\|\} \leq r$. Let $u = u_\theta$ be the neural network arising from the parameters θ , and let $v = v_{\tilde{\theta}}$ be the neural network arising from the parameters $\tilde{\theta}$. The difference in the output of the final layers of the neural network is

$$\begin{aligned} u(x) - v(x) &= b_1^{(n+1)} - \tilde{b}_1^{(n+1)} + \sum_{j=1}^{N^{(n)}} w_{1,j}^{(n+1)} \zeta(f_j^{(n)}(x)) - \sum_{j=1}^{N^{(n)}} \tilde{w}_{1,j}^{(n+1)} \zeta(\tilde{f}_j^{(n)}(x)) \\ &= b_1^{(n+1)} - \tilde{b}_1^{(n+1)} + \sum_{j=1}^{N^{(n)}} \left(w_{1,j}^{(n+1)} - \tilde{w}_{1,j}^{(n+1)}\right) \zeta(f_j^{(n)}(x)) \\ &\quad + \sum_{j=1}^{N^{(n)}} \tilde{w}_{1,j}^{(n+1)} \left(\zeta(f_j^{(n)}(x)) - \zeta(\tilde{f}_j^{(n)}(x))\right) \end{aligned}$$

where the functions within the neural network defined by $\tilde{\theta}$ are distinguished by a tilde on each of them. We can bound the squared difference by

$$\begin{aligned} \frac{1}{2} (u(x) - v(x))^2 &\leq \left(b_1^{(n+1)} - \tilde{b}_1^{(n+1)} + \sum_{j=1}^{N^{(n)}} \left(w_{1,j}^{(n+1)} - \tilde{w}_{1,j}^{(n+1)} \right) \zeta(f_j^{(n)}(x)) \right)^2 \\ &\quad + \left(\sum_{j=1}^{N^{(n)}} \tilde{w}_{1,j}^{(n+1)} \left(\zeta(f_j^{(n)}(x)) - \zeta(\tilde{f}_j^{(n)}(x)) \right) \right)^2 \end{aligned}$$

and using the CSI further by

$$\begin{aligned}
&\leq \left(\left(b_1^{(n+1)} - \tilde{b}_1^{(n+1)} \right)^2 + \sum_{j=1}^{N^{(n)}} \left(w_{1,j}^{(n+1)} - \tilde{w}_{1,j}^{(n+1)} \right)^2 \right) \cdot \left(1 + \sum_{j=1}^{N^{(n)}} \zeta(f_j^{(n)}(x))^2 \right) \\
&\quad + \left(\sum_{j=1}^{N^{(n)}} \left(\zeta(f_j^{(n)}(x)) - \zeta(\tilde{f}_j^{(n)}(x)) \right)^2 \right) \cdot \left(\sum_{j=1}^{N^{(n)}} \left(\tilde{w}_{1,j}^{(n+1)} \right)^2 \right) \\
&\leq \left(\left(b_1^{(n+1)} - \tilde{b}_1^{(n+1)} \right)^2 + \sum_{j=1}^{N^{(n)}} \left(w_{1,j}^{(n+1)} - \tilde{w}_{1,j}^{(n+1)} \right)^2 \right) \cdot K(r, x, n) \\
&\quad + \left(\sum_{j=1}^{N^{(n)}} \left(f_j^{(n)}(x) - \tilde{f}_j^{(n)}(x) \right)^2 \right) \cdot r^2 \\
&\leq \|\theta^{(n+1)} - \tilde{\theta}^{(n+1)}\|_{\ell^2}^2 \cdot K(r, x, n) + \left(\sum_{j=1}^{N^{(n)}} \left(f_j^{(n)}(x) - \tilde{f}_j^{(n)}(x) \right)^2 \right) \cdot r^2,
\end{aligned}$$

where the last inequality assumes $1 + \sum_j \zeta(f_j^{(n)}(x))^2 \leq K(r, x, n)$, which will be verified next, and also uses the bound $\max\{\|\theta\|, \|\tilde{\theta}\|\} \leq r$. In (60) it was shown that

$$\begin{aligned}
1 + \sum_{j=1}^{N^{(n)}} \zeta(f_j^{(n)}(x))^2 &\leq 1 + \sum_{j=1}^{N^{(n)}} (f_j^{(n)}(x))^2 = 1 + \|f_{1:N^{(n)}}^{(n)}(x)\|_2^2 \\
&\leq 1 + (n + \|x\|^2) \cdot (1 + \|\theta\|_{\ell^2}^{2n}) \leq K(r, x, n)
\end{aligned}$$

by setting $K(r, x, n) := 1 + (n + \|x\|^2) \cdot (1 + r^{2n})$.

The decomposition thus far articulates how $(u(x) - v(x))^2$ depends on the difference of the weights and biases of the output layer (layer $n + 1$). We may similarly articulate how $\sum_j (f_j^{(n)}(x) - \tilde{f}_j^{(n)}(x))^2$ depends on the difference of the weights and biases of the previous layers. For example,

$$\begin{aligned}
\frac{1}{2} \left(f_i^{(n)}(x) - \tilde{f}_i^{(n)}(x) \right)^2 &= \frac{1}{2} \left(b_i^{(n)} - \tilde{b}_i^{(n)} + \sum_{j=1}^{N^{(n-1)}} w_{i,j}^{(n)} \zeta(f_j^{(n-1)}(x)) - \tilde{w}_{i,j}^{(n)} \zeta(\tilde{f}_j^{(n-1)}(x)) \right)^2 \\
&\leq \left(\left(b_i^{(n)} - \tilde{b}_i^{(n)} \right)^2 + \sum_{j=1}^{N^{(n-1)}} \left(w_{i,j}^{(n)} - \tilde{w}_{i,j}^{(n)} \right)^2 \right) \cdot \left(1 + \sum_{j=1}^{N^{(n-1)}} \left(f_j^{(n-1)}(x) \right)^2 \right) \\
&\quad + \left(\sum_{j=1}^{N^{(n-1)}} \left(f_j^{(n-1)}(x) - \tilde{f}_j^{(n-1)}(x) \right)^2 \right) \cdot \left(\sum_{j=1}^{N^{(n-1)}} \left(\tilde{w}_{i,j}^{(n)} \right)^2 \right),
\end{aligned}$$

and summing over i gives

$$\begin{aligned}
& \frac{1}{2} \sum_{i=1}^{N^{(n)}} \left(f_i^{(n)}(x) - \tilde{f}_i^{(n)}(x) \right)^2 \\
& \leq \sum_{i=1}^{N^{(n)}} \left(\left(b_i^{(n)} - \tilde{b}_i^{(n)} \right)^2 + \sum_{j=1}^{N^{(n-1)}} \left(w_{i,j}^{(n)} - \tilde{w}_{i,j}^{(n)} \right)^2 \right) \cdot \left(1 + \sum_{j=1}^{N^{(n-1)}} \left(f_j^{(n-1)}(x) \right)^2 \right) \\
& \quad + \left(\sum_{j=1}^{N^{(n-1)}} \left(\left(f_j^{(n-1)}(x) - \tilde{f}_j^{(n-1)}(x) \right)^2 \right) \right) \cdot \sum_{i=1}^{N^{(n)}} \left(\sum_{j=1}^{N^{(n-1)}} \left(\tilde{w}_{i,j}^{(n)} \right)^2 \right) \\
& \leq \sum_{i=1}^{N^{(n)}} \left(\left(b_i^{(n)} - \tilde{b}_i^{(n)} \right)^2 + \sum_{j=1}^{N^{(n-1)}} \left(w_{i,j}^{(n)} - \tilde{w}_{i,j}^{(n)} \right)^2 \right) \cdot K(r, x, n-1) \\
& \quad + \left(\sum_{j=1}^{N^{(n-1)}} \left(\left(f_j^{(n-1)}(x) - \tilde{f}_j^{(n-1)}(x) \right)^2 \right) \right) \cdot r^2 \\
& \leq \|\theta^{(n)} - \tilde{\theta}^{(n)}\|_{\ell^2}^2 \cdot K(r, x, n-1) + \left(\sum_{j=1}^{N^{(n-1)}} \left(\left(f_j^{(n-1)}(x) - \tilde{f}_j^{(n-1)}(x) \right)^2 \right) \right) \cdot r^2.
\end{aligned}$$

In summary, we obtain $\frac{1}{2} (u(x) - v(x))^2 \leq \bar{K}(r, x, n) \|\theta - \tilde{\theta}\|_{\ell^2}^2$ for a constant \bar{K} depending only on r , x , and n . In particular, when $\tilde{\theta} = 0$ then $v = 0$, which implies $\frac{1}{2} (u(x))^2 \leq \bar{K}(r, x, n) \|\theta\|_{\ell^2}^2$.

We conclude the proof similarly to the proof of Theorem 2. Assume that $\max\{\|\theta\|_{\ell^2}, \|\tilde{\theta}\|_{\ell^2}\} < r$, so that $\max_j |u_j| \leq r \sqrt{2 \max_j \{ \bar{K}(r, \mathcal{T}(x, j), n) \}}$ and $\max_j |v_j| \leq r \sqrt{2 \max_j \{ \bar{K}(r, \mathcal{T}(x, j), n) \}}$. Then using the mean value theorem, we note that for any \bar{r} there exists a constant $C(\bar{r})$, such that for any vectors $u_{1:M}, v_{1:M}$ with $\max_j |u_j| \leq \bar{r}$, $\max_j |v_j| \leq \bar{r}$ we have

$$\begin{aligned}
| \ell(y|u, \sigma) - \ell(y|v, \sigma) | & \leq C(\bar{r}) \cdot \left(|u_1 - v_1|^2 + \dots + |u_M - v_M|^2 \right)^{\frac{1}{2}} \\
& = C(\bar{r}) \cdot \left(\sum_{j=1}^M (u(\mathcal{T}(x, j)) - v(\mathcal{T}(x, j)))^2 \right)^{\frac{1}{2}} \\
& \leq \sqrt{2} C(\bar{r}) \cdot \left(\sum_{j=1}^M \bar{K}(r, \mathcal{T}(x, j), n) \right)^{\frac{1}{2}} \cdot \|\theta - \tilde{\theta}\|_{\ell^2}.
\end{aligned}$$

The result holds by choosing $\bar{r} = r \sqrt{2 \max_j \bar{K}(r, \mathcal{T}(x, j), n)}$. \square

B.6. Proof of Theorem 4.

Proof of Theorem 4. The equivalence of $\mathcal{N}(\mathcal{CD}\ell(u), \mathcal{C}) \simeq \mathcal{N}(0, \mathcal{C})$ μ_0 -almost surely for all u will be shown by applying the Feldman-Hajek theorem [11, Theorem 2.23] which states that two Gaussian measures $\mathcal{N}(m_1, Q)$ and $\mathcal{N}(m_2, Q)$ are absolutely continuous with respect to one another if and only if $m_1 - m_2 \in Q^{1/2}(\mathcal{H})$ or $\sum_i (m_{1i} - m_{2i})^2 / \lambda_i^2 < \infty$ [11] where λ_i^2 are

the eigenvalues of \mathcal{Q} . For $m_1 = \mathcal{CD}\ell(u)$, $m_2 = 0$, and $\mathcal{Q} = \mathcal{C}$, this means showing

$$(61) \quad \sum_{i=1}^{\infty} \frac{(\mathcal{CD}\ell(u))_i^2}{\lambda_i^2} = \sum_{i=1}^{\infty} \frac{\lambda_i^4 (\mathcal{D}\ell(u))_i^2}{\lambda_i^2} = \sum_{i=1}^{\infty} \lambda_i^2 (\mathcal{D}\ell(u))_i^2$$

is finite for μ_0 -almost all u [11]. Note that $\mathcal{D}\ell(u)$ is the collection of partial derivatives with respect to each weight and bias parameter of the neural network. We will show that the sequence of truncated sums of (61) defines a submartingale that converges μ_0 -almost surely to a random variable with finite expectation.

We now specify the limiting neural network. As $\alpha > 1$, we have μ_0 -almost surely, $\|W_{1,:}^{(n+1)}\|^2 + \|B^{(n+1)}\|^2 + \sum_{l=1}^n \|W_{:,l}\|^2 + \|B^{(l)}\|^2 < \infty$. The limiting neural network is thus defined to be, for $l > 1$, $f_i^{(l)} = \langle (1, \zeta(f_i^{(l-1)}), (B_i^{(l)}, W_{i,:}^{(l)})) \rangle_{\ell^2}$. Indeed $\sum_{i=1}^{\infty} (f_i^{(l)})^2 < \infty$ and thus the definition is recursive.

Substituting both the eigenvalues of \mathcal{C} and the derivatives with respect to the parameters of the neural network into Equation (61) and truncating the sum gives

$$(62) \quad \begin{aligned} S_s = & \sigma_{b^{(n+1)}}^2 \left(\frac{\partial \ell}{\partial B_1^{(n+1)}} \right)^2 + \sum_{j=1}^s \frac{\sigma_{w^{(n+1)}}^2}{j^\alpha} \left(\frac{\partial \ell}{\partial W_{1,j}^{(n+1)}} \right)^2 \\ & + \sum_{l=2}^n \sum_{i=1}^s \left[\frac{\sigma_{b^{(l)}}^2}{i^\alpha} \left(\frac{\partial \ell}{\partial B_i^{(l)}} \right)^2 + \sum_{j=1}^s \frac{\sigma_{w^{(l)}}^2}{(ij)^\alpha} \left(\frac{\partial \ell}{\partial W_{i,j}^{(l)}} \right)^2 \right] \\ & + \sum_{i=1}^s \left[\frac{\sigma_{b^{(1)}}^2}{i^\alpha} \left(\frac{\partial \ell}{\partial B_i^{(1)}} \right)^2 + \sum_{j=1}^d \frac{\sigma_{w^{(1)}}^2}{i^\alpha} \left(\frac{\partial \ell}{\partial W_{i,j}^{(1)}} \right)^2 \right]. \end{aligned}$$

For the likelihood ℓ in (29) and $T = 1$, we will show that $\lim_{s \rightarrow \infty} S_s$ exists and is finite μ_0 -almost surely so that the equivalence $\mathcal{N}(\mathcal{CD}\ell(u), \mathcal{C}) \simeq \mathcal{N}(0, \mathcal{C})$ follows (in fact we will show that S_s converges to a L^1 random variable as $s \rightarrow \infty$); the case for $T > 1$ follows similarly.

To this end, observe that under the assumption of uniformly bounded partial derivatives of $\ell(a, \cdot)$ for all a , each partial derivative can be further bounded by

$$\left(\frac{\partial \ell}{\partial B_i^{(l)}} \right)^2 \leq M \times c_t \times \sum_{k=1}^M \left(\frac{\partial u(x_t^k)}{\partial B_i^{(l)}} \right)^2$$

where $\sqrt{c_t}$ is the bound of partial derivatives of $\ell(a_t, \cdot)$. We firstly calculate $\partial u / \partial W_{i,j}^{(l)}$ and $\partial u / \partial B_i^{(l)}$, for all (i, j, l) , where $u = u(x)$ is the output of the NN for an input $x \in \mathbb{R}^d$ - the input has been dropped for notational convenience. These derivatives can be cast as derivatives of $\partial u / \partial g_i^{(l)}$ since u can be regarded as a function of $(g_1^{(l)}, g_2^{(l)}, \dots)$ and only $g_i^{(l)}$ is a function of $W_{i,j}^{(l)}$ and $B_i^{(l)}$, that is $g_i^{(l)} = \zeta(f_i^{(l)})$ and $f_i^{(l)} = B_i^{(l)} + \sum_k W_{i,k}^{(l)} g_k^{(l-1)}$. Thus

$$(63) \quad \frac{\partial u}{\partial W_{i,j}^{(l)}} = \frac{\partial u}{\partial g_i^{(l)}} \times \frac{\partial g_i^{(l)}}{\partial f_i^{(l)}} \times \frac{\partial f_i^{(l)}}{\partial W_{i,j}^{(l)}}, \quad \frac{\partial u}{\partial B_i^{(l)}} = \frac{\partial u}{\partial g_i^{(l)}} \times \frac{\partial g_i^{(l)}}{\partial f_i^{(l)}}.$$

The next step is obtain a bound on $\partial u/\partial g_k^{(l)}$ for all (l, k) . To this end, assume all $\partial u/\partial g_k^{(l+1)}$ for $k = 1, 2, \dots$ are available. The aim is to find $\partial u/\partial g_k^{(l)}$ (for all k) at the previous layer l :

$$\begin{aligned}
\frac{\partial u}{\partial g_k^{(l)}} &= \sum_{j=1}^{\infty} \frac{\partial u}{\partial g_j^{(l+1)}} \frac{\partial g_j^{(l+1)}}{\partial g_k^{(l)}} \\
&= \sum_{j=1}^{\infty} \frac{\partial u}{\partial g_j^{(l+1)}} \frac{\partial \zeta(f_j^{(l+1)})}{\partial f_j^{(l+1)}} \frac{\partial f_j^{(l+1)}}{\partial g_k^{(l)}} \\
(64) \quad &= \sum_{j=1}^{\infty} \frac{\partial u}{\partial g_j^{(l+1)}} \times \frac{\partial \zeta(f_j^{(l+1)})}{\partial f_j^{(l+1)}} \times W_{j,k}^{(l+1)}.
\end{aligned}$$

Using Assumption 9, we will employ the following non-negative upper bound $D_k^{(l)}$ for $\partial u/\partial g_k^{(l)}$, defined recursively as follows

$$\begin{aligned}
D_k^{(n)} &:= \left| W_{1,k}^{(n+1)} \right|, \\
(65) \quad D_k^{(l)} &:= \sum_{j=1}^{\infty} D_j^{(l+1)} \times \left| W_{j,k}^{(l+1)} \right|, \quad l = n-1, \dots, 1
\end{aligned}$$

(These can be shown to be finite bounds as follows: firstly by the Cauchy-Schwarz inequality (CSI) we have $D_k^{(n-1)} = \langle D_j^{(n)}, |W_{:,k}^{(n)}| \rangle_{\ell^2} \leq \|W_{1,:}^{(n+1)}\| \times \|W_{:,k}^{(n)}\|$. Also, it is square summable since $\sum_{k=1}^{\infty} (D_k^{(n-1)})^2 \leq \|W_{1,:}^{(n+1)}\|^2 \times \|W_{:,k}^{(n)}\|^2$. The remaining terms $D_k^{(l)}$ for $l < n-1$ can be studied similarly.)

Note that $D_k^{(l)}$ is independent of the collection of random variables $\{W_{i,j}^{(m)} : m \leq l, \forall i, \forall j\}$, a property we will call on repeatedly in the study of the moments. Using, $D_k^{(l)} = \lim_{s \rightarrow \infty} \sum_{j=1}^s D_j^{(l+1)} |W_{j,k}^{(l+1)}|$, we have

$$\left(D_k^{(l)} \right)^2 = \left(\lim_{s \rightarrow \infty} \sum_{j=1}^s D_j^{(l+1)} |W_{j,k}^{(l+1)}| \right)^2 = \lim_{s \rightarrow \infty} \left(\sum_{j=1}^s D_j^{(l+1)} |W_{j,k}^{(l+1)}| \right)^2$$

and thus

$$\mathbb{E} \left\{ \left(D_k^{(l)} \right)^2 \right\} = \lim_{s \rightarrow \infty} \mathbb{E} \left\{ \left(\sum_{j=1}^s D_j^{(l+1)} |W_{j,k}^{(l+1)}| \right)^2 \right\} = C_l k^{-\alpha}$$

where the final result of $C_l k^{-\alpha}$ will be established now. Squaring the finite sum in the expectation gives

$$\sum_{j=1}^s \left(D_j^{(l+1)} |W_{j,k}^{(l+1)}| \right)^2 + 2 \sum_{j=1}^s \sum_{i=j+1}^s \left(D_j^{(l+1)} |W_{j,k}^{(l+1)}| \right) \left(D_i^{(l+1)} |W_{i,k}^{(l+1)}| \right).$$

The expected value of the cross term can be bounded by

$$\begin{aligned}
&\sum_{j=1}^s \sum_{i=j+1}^s \sqrt{\mathbb{E} \left[\left(D_j^{(l+1)} W_{j,k}^{(l+1)} \right)^2 \right]} \sqrt{\mathbb{E} \left[\left(D_i^{(l+1)} W_{i,k}^{(l+1)} \right)^2 \right]} \\
&= \sum_{j=1}^s \sum_{i=j+1}^s \sqrt{\mathbb{E} \left[\left(D_j^{(l+1)} \right)^2 \right]} \sqrt{\mathbb{E} \left[\left(W_{j,k}^{(l+1)} \right)^2 \right]} \sqrt{\mathbb{E} \left[\left(D_i^{(l+1)} \right)^2 \right]} \sqrt{\mathbb{E} \left[\left(W_{i,k}^{(l+1)} \right)^2 \right]}
\end{aligned}$$

due to the independence of $D_j^{(l+1)}$ and $W_{j,k}^{(l+1)}$. The expected value of the sum of squares term can be similarly upper bounded by

$$\sum_{j=1}^s \mathbb{E} \left[\left(D_j^{(l+1)} |W_{j,k}^{(l+1)}| \right)^2 \right] = \sum_{j=1}^s \mathbb{E} \left[\left(D_j^{(l+1)} \right)^2 \right] \mathbb{E} \left[\left(|W_{j,k}^{(l+1)}| \right)^2 \right].$$

For $l = n - 1$, substituting the definitions above gives

$$\sum_{j=1}^s \mathbb{E} \left[\left(D_j^{(n)} |W_{j,k}^{(n)}| \right)^2 \right] = \sum_{j=1}^s \mathbb{E} \left[\left(W_{1,j}^{(n+1)} W_{j,k}^{(n)} \right)^2 \right] = k^{-\alpha} \sigma_{w^{(n+1)}}^2 \sigma_{w^{(n)}}^2 \sum_{j=1}^s j^{-2\alpha}.$$

For the cross terms, we get

$$\sum_{j=1}^s \sum_{i=j+1}^s \sqrt{\mathbb{E} \left[\left(D_j^{(n)} W_{j,k}^{(n)} \right)^2 \right]} \sqrt{\mathbb{E} \left[\left(D_i^{(n)} W_{i,k}^{(n)} \right)^2 \right]} = k^{-\alpha} \sigma_{w^{(n+1)}}^2 \sigma_{w^{(n)}}^2 \sum_{j=1}^s \sum_{i=j+1}^s j^{-\alpha} i^{-\alpha}.$$

Thus $\mathbb{E} \left[\left(\partial v / \partial g_k^{(n-1)} \right)^2 \right] \leq \mathbb{E} \left[\left(D_k^{(n-1)} \right)^2 \right] = C_{n-1} k^{-\alpha}$, where the constant C_{n-1} does not depend on s . The result can be extrapolated to all $l < n$ by induction over the layer index to get

$$(66) \quad \mathbb{E} \left[\left(\frac{\partial u}{\partial g_k^{(l)}} \right)^2 \right] \leq \mathbb{E} \left[\left(D_k^{(l)} \right)^2 \right] = C_l k^{-\alpha}$$

for all $x \in \mathcal{X}$. Combining (63) and (66) and using Assumption 9 as well as Theorem 1 gives

$$\mathbb{E} \left[\left(\frac{\partial u}{\partial W_{i,j}^{(l)}} \right)^2 \right] \leq \mathbb{E} \left[\left(\frac{\partial u}{\partial g_i^{(l)}} \right)^2 \left(\frac{\partial f_i^{(l)}}{\partial W_{i,j}^{(l)}} \right)^2 \right] \leq \mathbb{E} \left[\left(D_i^{(l)} \right)^2 \right] \mathbb{E} \left[\left(g_j^{(l-1)} \right)^2 \right] \leq C_l i^{-\alpha} \sigma_{l-1}^2 j^{-\alpha}$$

for all $x \in \mathcal{X}$, for constants C_l not depending on s . Similarly, $\mathbb{E} \left[\left(\partial u / \partial B_i^{(l)} \right)^2 \right] \leq \mathbb{E} \left[\left(\partial u / \partial g_i^{(l)} \right)^2 \right] \leq C_l i^{-\alpha}$. Bringing together these results gives the following bound for $\mathbb{E}(S_s)$ in (62)

$$\begin{aligned} \mathbb{E}(S_s) &\leq c_t M^2 \times \left[\sigma_{b^{(n+1)}}^2 C_{n+1} + \sum_{j=1}^s \frac{\sigma_{w^{(n+1)}}^2}{j^\alpha} C_{n+1} \sigma_n^2 j^{-\alpha} \right] \\ &\quad + c_t M^2 \times \sum_{l=2}^n \sum_{i=1}^s \left[\frac{\sigma_{b^{(l)}}^2}{i^\alpha} C_l i^{-\alpha} + \sum_{j=1}^s \frac{\sigma_{w^{(l)}}^2}{(ij)^\alpha} C_l i^{-\alpha} \sigma_{l-1}^2 j^{-\alpha} \right] \\ &\quad + c_t M^2 \times \sum_{i=1}^s \left[\frac{\sigma_{b^{(1)}}^2}{i^\alpha} C_1 i^{-\alpha} + \sum_{j=1}^d \frac{\sigma_{w^{(1)}}^2}{i^\alpha} C_1 i^{-\alpha} x_j^2 \right]. \end{aligned}$$

As S_s is a submartingale and its mean is bounded uniformly in s . By the martingale convergence theorem, it converges almost surely to an L^1 random variable and thus the result follows. \square

APPENDIX C. DETAILS ON EXPERIMENTAL SETUP

We here give further details on the experimental setup for the Examples 5.1. Both examples are included in the python package ‘gym’ [7].

C.1. Mountaincar. The first example is the popular mountaincar problem. The state space is the 2-dimensional domain $\mathcal{X} = [-1.2, 0.6] \times [-0.07, 0.07]$, where the first variable is the position x_1 of the car on a mountain slope, and the second variable represents its velocity x_2 . The set of possible actions is $\mathcal{A} = \{-1, 0, 1\}$, representing exerting force to the left, not adding force, and exerting force to the right, respectively. The state transitions are deterministic, being given by Newtonian physics, and we refer the reader to the OpenAI documentation or to our code for the details.

In the mountaincar problem, the reward is constant $r(x_1, x_2) = -1$ per step, until the car reaches the top of the mountain ($x_1 \geq 0.5$). The optimal policy is therefore to reach the mountaintop as quickly as possible. An optimal deterministic policy [55] is given by

$$\begin{aligned} \mu(x_1, x_2) = -1 + 2\mathbb{I}\{\min(-0.09(x_1 + 0.25)^2 + 0.03, 0.3(x_1 + 0.9)^4 - 0.008) \leq x_2 \\ \leq -0.07(x_1 + 0.38)^2 + 0.07\}, \end{aligned}$$

and we generated state-action pairs by firstly drawing a random initial state in the valley of the mountain, $x \sim \mathcal{U}([-0.6, -0.4])$, i.e. a uniform value between -0.6 and -0.4 . The initial velocity is set to 0. Starting from that state, we computed the action given the optimal policy given above. Once the flag was reached, a new initial state was drawn, and the process repeated until we had a total of 250 observations. This gave a set of state-action pairs $\{(x_t, a_t)\}_{t=1}^{250}$, and we then took every fifth sample to obtain the final dataset $y = \{(x_{5t}, a_{5t})\}_{t=1}^{50}$. This resulted in the state variables in y covering the entire state space, such that we can expect to learn the value function in any region an agent might find themselves in. The likelihood (22) arises from this dataset y and the noise level being set to $\sigma = 0.1$.

In the simulations from the learned value functions, we again initialised the state variable as $x \sim \mathcal{U}([-0.6, -0.4])$ and set the velocity to 0. We then simulated noise and used Equation (19) with the learned value function to pick an action. In Section 5.3, the used value function was taken as either a sample from the posterior or as the mean function; in Section 5.4 the used value function was the mean function from the posteriors. In all experiments, if the car didn't make it to the flag within 200 time steps, we called this a failure and restarted the process from new initial conditions.

C.2. HalfCheetah. To show that our algorithm works in a more complicated setting, we looked at the HalfCheetah example from the MuJoCo library [49] where the state x_t a 17-dimensional vector. The original continuous actions space of the problem is 6-dimensional.

An agent controlling the cheetah is to move it to forward while not exerting too much force: positive rewards are given for moving forward, and negative rewards are given for moving backwards, a further penalty is deducted for actions requiring a lot of force. A black box optimal policy for the HalfCheetah problem was provided in Berkeley's Deep Reinforcement Learning Course⁷, which we used to simulate state-action pairs.

The initial state and velocity variables were drawn at random with distributions according to the python package 'gym' [7]. We discretised the action space to M actions in the following way: an initial state was drawn, and the black box policy gave us an action, taking us to a new state via deterministic mapping. Iterating this process, the first M actions were stored. From now on, we can use a discrete action space \mathcal{A}_M consisting of these M actions: at a state x_t we compute a_t as the action in \mathcal{A}_M that minimises the Euclidean distance to the action computed by the black box policy. We found that $M = 8$ actions were sufficient to get behaviour very similar to the one we got when using the

⁷CS294-112 HW 1: Imitation Learning, <https://github.com/berkeleydeeprlcourse/homework/tree/master/hw1>

continuous action space, and we thus fixed $\mathcal{A} = \mathcal{A}_8$. We refer to the action $a \in \mathcal{A}$ that minimises the Euclidean distance to the black box algorithm as ‘optimal’. To generate data, we firstly drew an initial state x_1 , and then computed the optimal action a_1 using the procedure just described, and computed the next state using the state dynamics (16). After 25 steps, we restarted from a new initial state, and repeated this process another 4 times until we had a total of $T = 100$ data points. The reason we restarted occasionally was, as in the mountaincar example, to ensure that we cover a representative region of the state space. The dataset $y = \{(x_t, a_t)\}_{t=1}^{100}$ was used in the likelihood (22), where we set the noise level to $\sigma = 0.1$. In the experiments in Section 5.4, an initial state is drawn, and the cheetah is controlled using Equation (19) over 100 time steps.